JOURNAL OF GEOPHYSICAL RESEARCH, VOL. 114, B05406, doi:10.1029/2008JB005866, 2009

Clay fabric intensity in natural and artificial fault gouges: Implications for brittle fault zone processes and sedimentary basin clay fabric evolution

Samuel H. Haines,[1] Ben A. van der Pluijm,[1] Matt J. Ikari,[2] Demian M. Saffer,[2] and Chris Marone[2]

Received 12 June 2008; revised 22 November 2008; accepted 2 February 2009; published 13 May 2009.

[1] The role of phyllosilicate fabrics in fault gouge is a poorly understood component of the mechanical and hydrologic behavior of brittle fault zones. We present 90 fabric intensity measurements using X-ray texture goniometry on 22 natural clay-rich fault gouges from low-angle detachment faults (Death Valley area detachments, California; Ruby Mountains, Nevada; West Salton Detachment Fault, California) and the Peramola thrust in NE Spain. Natural fault gouges have uniformly weak clay fabrics (multiples of a random distribution (MRD) = 1.7–4.5, average MRD = 2.6) when compared to phyllosilicate-rich rocks found in other geologic settings. Clay fabric intensities in natural gouges do not vary significantly either as a function of tectonic environment or of dominant clay mineralogy in the gouge. We compare these natural samples with 69 phyllosilicate fabric intensities measured in laboratory experiments on synthetic clay-quartz mixtures. Clay fabric intensities from laboratory samples are similar to those in natural gouges (MRD = 1.7–4.6), but increase systematically with increasing shear strain and normal stress. Total phyllosilicate content does not significantly affect clay fabric intensity. Shear strain is important for developing stronger fabrics; samples subjected solely to compression exhibit uniformly weak fabrics (MRD = 1.6–1.8) even when compressed at high normal stresses (150 MPa). The weak fabrics found in natural fault gouge indicate that if anisotropic and overall low fault zone permeability allow elevated pore fluid pressures and fault weakening, this anisotropy must be a transient feature that is not preserved. Our data also reinforce the idea that clay fabric development in sedimentary rocks is primarily a function of authigenic mineral growth and not of compaction-induced particle rotation.

Citation: Haines, S. H., B. A. van der Pluijm, M. J. Ikari, D. M. Saffer, and C. Marone (2009), Clay fabric intensity in natural and artificial fault gouges: Implications for brittle fault zone processes and sedimentary basin clay fabric evolution, *J. Geophys. Res.*, *114*, B05406, doi:10.1029/2008JB005866.

1. Introduction

[2] Clay-rich fault gouges play a significant role in controlling the frictional and hydrologic properties of seismic and aseismic faults [e.g., *Sibson*, 1977; *Byerlee*, 1978; *Vrolijk and van der Pluijm*, 1999]. Although a large body of experimental data has quantified the frictional properties of clay-rich gouges [e.g., *Lupini et al.*, 1981; *Morrow et al.*, 1992, 2000; *Logan and Rauenzahn*, 1987; *Moore et al.*, 1989; *Saffer et al.*, 2001; *Brown et al.*, 2003; *Saffer and Marone*, 2003; *Numelin et al.*, 2007; *Ikari et al.*, 2007], the relationships between preferred alignment of clays, permeability, frictional stability, and fault strength are not well understood. The preferred orientation of phyllosilicates in natural faults has been suggested as a key control on fault frictional behavior [e.g., *Rice*, 1992]. Phyllosilicate preferred orientation has also been invoked to interpret slip rate and other in situ faulting conditions based on both surface exposures of preserved faults and scientific fault drilling [e.g., *Chester and Logan*, 1987; *Cladouhos*, 1999a, 1999b; *Cowan et al.*, 2003; *Storti et al.*, 2003; *Di Toro et al.*, 2005]. Quantifying the intensity and orientation of clay fabrics in clay-rich gouges is therefore important for assessing the degree to which clay fabrics in fault cores are anisotropic as would be required for maintaining a fluid pressure regime that is distinct from the surrounding wallrocks.

[3] Limited quantitative studies of clay fabric intensity in natural fault zones have shown that clay gouges generally have weak fabrics [*Yan et al.*, 2001; *Solum et al.*, 2003, 2005]. The goals of this paper are to (1) examine phyllo-

[1]Department of Geological Sciences, University of Michigan, Ann Arbor, Michigan, USA.
[2]Department of Geosciences and Energy Institute Center for Geomechanics, Geofluids, and Geohazards, Penn State University, University Park, Pennsylvania, USA.

0148-0227/09/2008JB005866$09.00

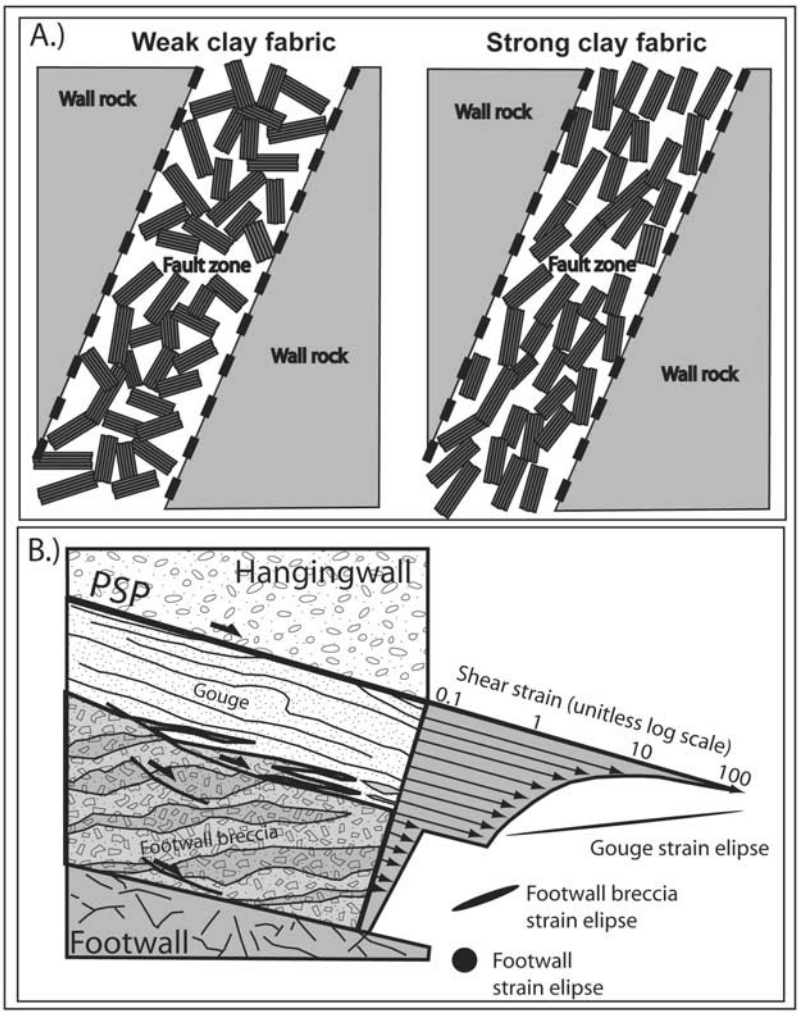

Figure 1. (a) Schematic illustration of clay fabric intensity (weak and strong clay fabrics) and orientation in fault zones. (b) Schematic illustration of low-angle normal fault zone architecture and strain distribution model of low-angle normal fault gouges of *Cowan et al.* [2003]. PSP is principal shear plane. Redrawn from *Cowan et al.* [2003].

silicate fabric intensities from natural clay-rich fault gouges in a variety of geologic environments, with a variety of clay minerals and (2) link the fabrics in natural gouges to those developed in synthetic gouges under controlled laboratory shearing experiments. The laboratory experiments are designed to assess the relative roles of normal stress, shear strain, and clay content on clay fabric intensity. We quantify clay gouge fabric intensity using X-ray texture goniometry (XTG). In this paper we focus on fabric measurements from low-angle normal faults and compare these with previously reported data for gouges from thrust faults, listric normal faults and strike slip faults. We examine natural gouges that contain predominantly illite, chlorite, smectite, kaolinite, palygorskite or sepiolite and assess the differences in fabric intensity of clay-rich gouges as a function of mineralogy and tectonic environment. Through the use of oriented specimens we link the orientation of clay fabric as determined by XTG to macroscopic fabrics visible in many fault gouges.

[4] Low-angle normal faults have long been of special interest as they apparently slip at very low dips compared to predictions from rock mechanics [e.g., *Buck*, 1988; *Wernicke and Axen*, 1988; *Axen*, 2004]. These faults have a recognizable geometry in the field, characterized by a highly asymmetric fault zone, with a brecciated and diffuse lower boundary and a reduction in grain and clast size approaching a relatively planer upper boundary surface [*Cladouhos*, 1999a; *Cowan*, 1999; *Cowan et al.*, 2003] (Figure 1). It has been proposed that the distribution of strain in low-angle normal faults is highly anisotropic and localized on an upper principal shear plane (PSP) at the contact of the gouge layer with the hangingwall. Moreover, strain apparently decreases exponentially across the gouge zone and into the damage zone in the footwall across a zone 2–20 m thick (Figure 1). As part of our study we test this concept by measuring clay fabric intensity in two sample transects across low-angle normal fault zones to ascertain if the posited increase in shear strain with proximity to the hanging wall contact is reflected in preferred alignment of clay minerals.

[5] To examine the processes that control the intensity and evolution of clay fabrics (Figure 1), we also conducted laboratory measurements of fabric intensity. This work

focuses on mixtures of montmorillonite and quartz, in order to evaluate the relative roles of normal stress, shear strain, and clay content. The experiments also permit an assessment of the degree to which strain in clay-rich mixtures is accommodated along discrete shear surfaces (''R'' surfaces of *Logan et al.* [1979]) or by bulk deformation and realignment of phyllosilicates. Moreover, simple compaction experiments provide an opportunity to evaluate sedimentary fabric development models such as the March strain model [*March*, 1932]. Although numerous conceptual models for clay compaction in sedimentary environments infer strong preferred orientation due to mechanical effects of compaction and consolidation [e.g., *Lambe*, 1953, 1958; *Ingles*, 1968; *Yong*, 1972], few experimental validations for this view have been offered [*Tullis*, 1976]. We aim to test the applicability of the March strain model [*March*, 1932] using clay-rich mixtures compressed at a variety of normal stresses. This work will test whether fabric can be used to quantify strain in clay-rich gouges and clay-rich sedimentary rocks.

2. Clay Fabric Intensity Measurements

[6] The preferred orientation of minerals in rock has typically been quantified using the following four techniques: (1) universal stage optical microscopy [e.g., *Turner and Weiss*, 1963], (2) semiautomated optical microscopy [e.g., *Price*, 1973; *Heilbronner and Pauli*, 1993], (3) electron backscattered diffraction [e.g., *Lloyd*, 1987; *Wilkinson and Hirsch*, 1997], and (4) X-ray texture goniometry [e.g., *Schulz*, 1949; *Oertel*, 1983; *van der Pluijm et al.*, 1994]. Additionally, bulk rock fabric quantification has been obtained by magnetic analysis [e.g., *Housen et al.*, 1993; *Richter et al.*, 1993; *Pares et al.*, 1999] and neutron diffraction [*Wenk*, 2006]. Because clay crystallite dimensions are typically a few microns or less, which is below the resolution of optical or scanning electron microscopy, X-ray texture goniometry is our preferred technique for quantifying clay fabric.

[7] XTG is ideal for the quantification of fabric intensity in clay-rich fault gouge because it provides information for large numbers of small particles in three dimensions, and the analysis and sample preparation are straightforward. The XTG technique has been used to quantify phyllosilicate fabric intensity in the following four basic areas: (1) Identifying the relative roles of compaction and authigenic mineral growth in the mud-to-shale transition [*Sintubin*, 1994b; *Curtis et al.*, 1980; *Ho et al.*, 1999; *Aplin et al.*, 2006; *Day-Stirrat et al.*, 2008]; (2) assessing the relative roles of mechanical rotation, dissolution, and neocrystallization of micas in the shale-to-slate transition [*Holeywell and Tullis*, 1975; *Tullis and Wood*, 1975; *Sintubin*, 1994a; *Ho et al.*, 1995, 1996, 2001; *Jacob et al.*, 2000]; (3) Assessing the symmetry of the preferred orientation of micas in phyllonitic and mylonitic rocks [*O'Brien et al.*, 1987]; and (4) Quantifying phyllosilicate fabric intensities in clay-rich fault gouges [*Yan et al.*, 2001; *Solum et al.*, 2003, 2005; *Schleicher et al.*, 2009]. The technique has also been used to study spatial variations of strain, on the mm to m scale, in phyllosilicate-rich rocks [*Oertel and Curtis*, 1972; *Holeywell and Tullis*, 1975; *Curtis et al.*, 1980; *van der Pluijm et al.*, 1994; *Ho et al.*, 1995].

[8] Results of XTG measurements are typically expressed in multiples of a random distribution (MRD) units. which are analogous to % of the data per 1% area of the pole figure [*Wenk*, 1985], e.g., an MRD value of 3 means that 3% of the total corrected number of X-ray counts are found in 1% of the pole figure.

3. Faults Studied

[9] We measured fabric intensities of clay-rich gouges from nine faults. Six of these were detachment faults in the Death Valley, CA area (the Badwater, Copper Canyon, Mormon Point (2 exposures), Gregory Peak Detachments, the basal fault of the Amargosa Chaos, and a low-angle detachment exposed near the Dante's View overview in Death Valley NP). We also sampled gouge from 3 other faults, the Ruby Mountains detachment fault in NE Nevada (exposed at 2 localities, Secret Pass and Clover Hill), the Salton Detachment in SW California and the Peramola Thrust in NE Spain (Figure 2). We chose these faults to complement previous XTG studies on listric normal faults (Moab Fault, Utah, United States [*Solum et al.*, 2005]), thrust faults (Lewis Thrust, Alberta, Canada [*Yan et al.*, 2001]) and strike-slip faults (Punchbowl Fault, California, United States [*Solum et al.*, 2003]).

[10] Low-angle normal faults have received little attention for fabric quantification, yet they are of considerable interest due to the mechanical paradox of their shallow dip and misorientation relative to theoretical and laboratory predictions [e.g., *Buck*, 1988; *Wernicke and Axen*, 1988; *Axen*, 2004]. The Peramola thrust was included because the gouge contains significant corrensite (ordered chlorite/smectite), a mineral that has increasingly been identified in clay gouges in surface exposures and scientific drilling projects [e.g., *Schleicher et al.*, 2008; S. Haines, Transformations in clay-rich fault rocks: Constraining fault zone processes and the kinematic evolution of regions, University of Michigan, unpublished Ph.D. thesis, 2008].

3.1. Death Valley Area Low-Angle Normal Faults

[11] We sampled a total of seven localities in southern Death Valley, California. This area has exceptional exposure and preservation of clay-rich fault gouges along shallowly dipping NW-directed normal faults of Miocene-to-Recent age, and the faults have been studied extensively [*Pavlis et al.*, 1993; *Miller*, 1996; *Cladouhos*, 1999a, 1999b; *Cowan*, 1999; *Cowan et al.*, 2003; *Hayman et al.*, 2004; *Hayman*, 2006; Haines, unpublished thesis, 2008]. Sample localities included the three ''turtlebacks'' on the west side of the Black Mountains, one locality in the southern Black Mountains in the Amargosa Chaos area, and one locality at a smaller detachment in the central Black Mountains near Dante's View (see Figure 2 and Table 1). At all localities, the faults juxtapose poorly sorted, moderately indurated Pliocene-Recent gravels against either highly fractured and chloritized Precambrian metamorphic rocks (as at Badwater, Copper Canyon and Mormon-3) or fractured mid-Miocene dioritic and granitic plutonic rocks at Mormon-2 and Size 36 Canyon (the Gregory Peak detachment). The fault rocks of the Death Valley detachments have been described in detail by *Cladouhos* [1999a, 1999b], *Cowan et al.* [2003], and *Hayman et al.* [2004] and outcrop details are found given by Haines (unpublished thesis, 2008).

[12] In outcrop, the gouges commonly, but not always, have a crude foliation subparallel to the fault zone margins

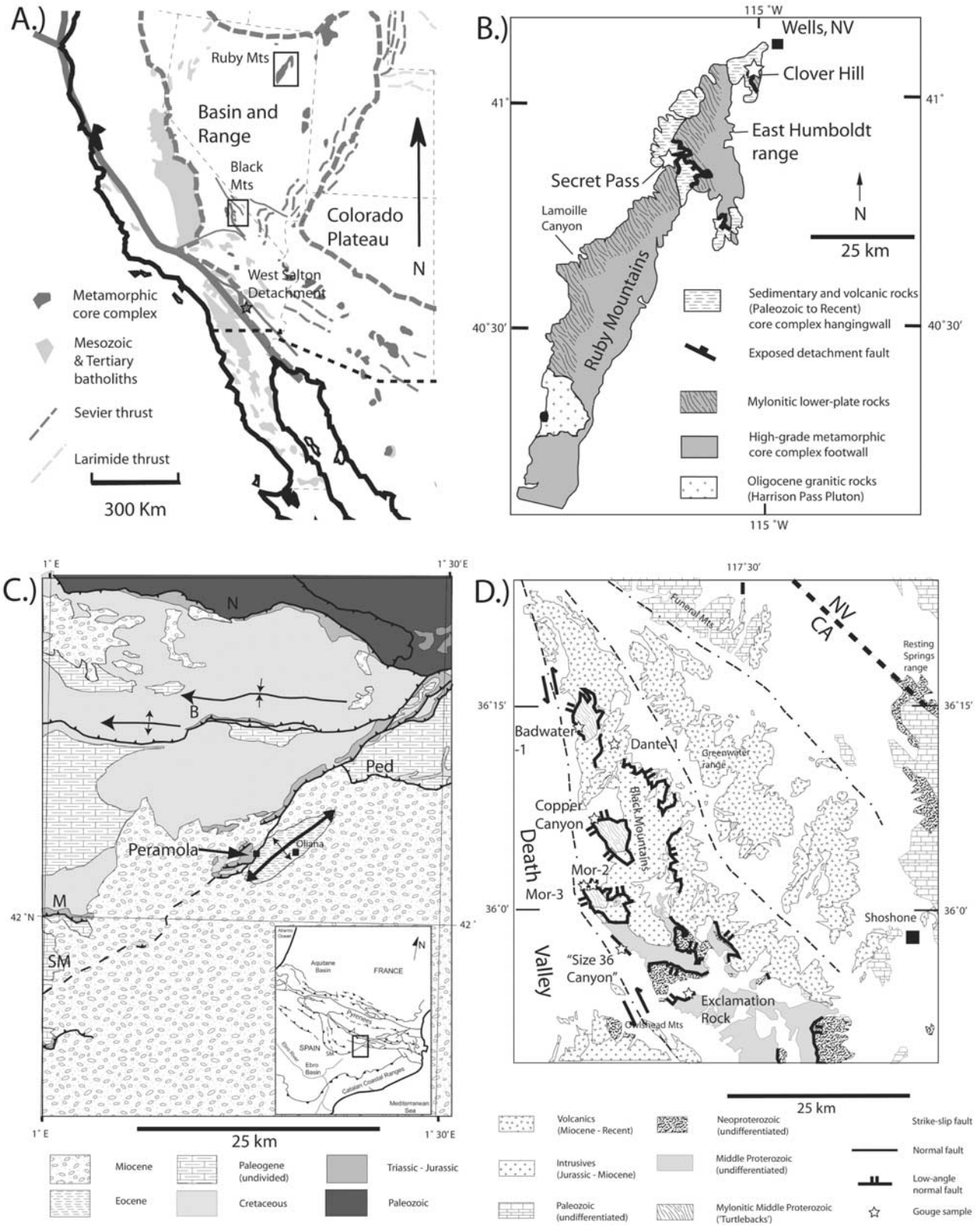

Figure 2. Location map for samples used in this study. (a) Schematic geologic map of the western United States showing major regional tectonic elements and detachment faults examined in this study (redrawn after *Coney* [1980]). Boxes indicate areas of Figures 2b and 2d. (b) Schematic geological map of the Ruby and East Humboldt Mountains, Nevada, indicating sample locations. (c) Sketch geologic map of the Pyrenees showing major thrust faults. SM, Serres Marginales thrust system; B, Boixols thrust; M, Montsec thrust; N, Nogueres thrust system; PED, Pedraforca Nappe. (d) Sketch geological map showing the central Black Mountains and Death Valley area, California, and sample locations.

Table 1. Location of Samples Used in This Study

Range	Fault	Sample Suite	Latitude	Longitude
Ruby Mountains, Nevada	Clover Hill	Clover	41° 3′ 48″N	115° 1′ 21″W
Ruby Mountains, Nevada	Secret Pass	Secret Pass	40° 51′ 53″N	115° 15′ 15″W
Black Mountains, California	Badwater-1	Badwater	36° 15′ 25″N	116° 46′ 29″W
Black Mountains, California	Copper Canyon	Copper Canyon	36° 7′ 28″N	116° 44′ 34″W
Black Mountains, California	Dante's View	Dante-1	36° 13′ 27″N	116° 42′ 39″W
Black Mountains, California	Mormon-2	Mormon-2	36° 2′ 37″N	116° 44′ 12″W
Black Mountains, California	Mormon-3	Mormon-3	36° 2′ 31″N	116° 44′ 20″W
Black Mountains, California	Size 36 Canyon	Size 36	35° 57′ 50″N	116° 40′ 34″W
Black Mountains, California	Exclamation Rock	Exclamation Rock	35° 55′ 11″N	116° 32′ 39″W
Santa Rosa Mountains, California	West Salton Detachment	Salton 571	33° 20′ 44″N	116° 8′ 12″
Pyrenees	Peramola Thrust	Peramola	42° 3′ 32″N	1° 15′ 43″E

defined by Y, R and P surfaces (using the terminology of *Chester et al.* [1985]). Gouge layers at all exposures range from 0.2 m to 2.0 m thick, and gouge zone thicknesses vary rapidly along strike. At Exclamation Rock on the Shoshone-Death Valley road, the Amargosa detachment places mid-Proterozoic Crystal Springs greenschist-facies quartzites over mid-Proterozoic muscovite schistose gneisses. On the road to Dante's View, (the fault at mile 11.3 of *Miller and Wright* [2004]), a low-angle normal fault juxtaposes Miocene rhyolites in the hangingwall over Miocene white tuff in the footwall.

[13] X-ray diffraction (XRD) analyses indicate that the Death Valley gouges are mineralogically variable (Haines, unpublished thesis, 2008). The gouges have two characteristic clay mineral assemblages; one is dominated by detrital chlorite and its alteration products, corrensite and smectite, derived from pervasive chloritic alteration of the footwall. The second assemblage is dominated by authigenic $1M_d$ illite, which is derived from the breakdown of feldspar in granitic footwall rocks. The distribution of the two assemblages is primarily a function of the distribution of footwall lithologies. At Mormon-3, a very distinctive gouge mineral assemblage of trioctahedral smectite, sepiolite, talc, and lizardite is found overprinting an apparently older detrital chloritic gouge based on field relationships. Field fabrics indicate that both assemblages predate the end of slip on the detachment. At Dante's View, the gouge contains a distinctive assemblage of dioctahedral smectite (montmorillonite) and palygorskite.

3.2. Ruby Mountains Detachment, Nevada

[14] The Ruby Mountains metamorphic core complex is a well studied structure in NE Nevada [e.g., *Snoke*, 1980; *Dallmeyer et al.*, 1986; *Dokka et al.*, 1986; *Mueller and Snoke*, 1993; *McGrew and Snee*, 1994; *McGrew et al.*, 2000]. The complex was exhumed along a west-dipping mylonitic detachment that is exposed sporadically along the western margin of the range and at Clover Hill at the northern end of the East Humboldt Range. The detachment has a ductile-to-brittle structural history, and was active from the Eocene to the late Miocene [*Dokka et al.*, 1986; *McGrew et al.*, 2000]. We sampled the detachment fault system gouges at two localities (see Figure 2 and Table 1), on NV Rt 321 approximately 5 km southwest of Wells, NV (Stop 20 of *Snoke and Howard* [1984]), where the detachment places Miocene conglomerates over mylonitic probable Cambro-Orovician metacarbonates and at Secret Pass where the main detachment fault is exposed along NV Route 229 (Stop 12, locality H of *Snoke and Howard* [1984]), where the detachment places Miocene zeolitized tuffs over silicified mylonitic probable Cambro-Orovician metacarbonates. At Clover Hill, the gouge zone is 1 m thick, reddish in color with white streaks along a crude fault-parallel foliation. XRD analysis of the gouge indicates that the Clover Hill gouge is dominated by illite, but that the white streaks are predominantly kaolinite, which likely postdates faulting, as the white streaks clearly cut across the predominant foliation in the gouge (Haines, unpublished thesis, 2008). At Secret Pass, the gouge zone of the main detachment fault is 1.0–1.5 m thick and XRD analysis indicates that the gouge contains discrete horizons of illite-rich illite-smectite (~90% I in I/S) and dioctahedral smectite. The illite-smectite is crudely foliated subparallel to the fault plane at outcrop, and thus was present during the last slip event, whereas the smectite is not visibly foliated and may postdate fault slip (Haines, unpublished thesis, 2008).

3.3. West Salton Detachment Fault

[15] The West Salton Detachment Fault is one of a suite of east-dipping low-angle normal faults on the western side of the Miocene-to-Recent Salton Trough, which forms the northern end of the Gulf of California. The fault was sampled in a small wash in the Santa Rosa Mountains (33° 20′ 44″N, 116° 8′ 12″W), where the detachment juxtaposes Paleozoic greenschist- and amphibolite-facies metasediments in both the hangingwall and footwall. The fault strikes roughly NW-SE and accommodated ESE-directed extension from the Miocene to early Pleistocene [*Axen and Fletcher*, 1998]. Locally, the fault strikes NE-SW and dips ~25° to the east. The gouge zone is 0.25 to 0.5 m thick and displays a weak platy fabric subparallel to the fault plane. XRD analysis of the gouge shows that it consists primarily of a trioctahedral smectite (saponite) and chlorite (Haines, unpublished thesis, 2008).

3.4. Peramola Thrust, Spain

[16] The Peramola thrust in the south-central Spanish Pyrenees is part of the Serres Marginals frontal thrust system. The thrust is exposed in a small roadcut (42° 3′ 32″N, 1° 15′ 43″E) at the village of Peramola, near the eastern termination of the Serres Marginals thrust system, where the fault places mid-Jurassic limestones over Eocene marls along the northwest margin of the Oliana anticline. The fault was active in the late Eocene during emplacement of the south-central Pyrenean thrust wedge [*Puigdefàbregas et al.*, 1986; *Sussman et al.*, 2004]. Locally, the thrust strikes NNW and dips west at 35°. The gouge zone is 2–3 m thick and is weakly foliated subparallel to the fault zone margins at outcrop. XRD analysis of the gouge indicates that it consists

of corrensite (ordered chlorite-smectite) and minor illite (S. H. Haines, unpublished thesis, 2008).

[17] We characterized the clay mineral assemblages in all sampled gouges in detail by conventional XRD. These data indicate that with the exception of detrital chlorite in the Death Valley and West Salton Detachment Fault, clays are predominantly authigenic in origin and are not composed of detrital material derived from the wall rock (Haines, unpublished thesis, 2008). For the faults sampled in this study, most clay gouges were volumetrically dominated by one or at most two clay minerals, with only minor abundances of other clays. None of the faults we sampled had significant veining or other visible evidence at outcrop of high fluid pressures.

4. Methods for X-Ray Texture Goniometry

4.1. Sampling of Gouge From Natural and Laboratory Faults

[18] We sampled gouge using a variety of field techniques and preservation methods. Natural samples were oriented with respect to the fault zone and either chiseled out of the fault zone or carefully removed along existing fractures using a pocketknife. Laboratory gouge layers were oriented relative to the shear direction and carefully removed from the shear forcing blocks [e.g., *Ikari et al.*, 2007]. Both sets of gouge samples were set in a low viscosity epoxy (Struers EPOFIX) under low vacuum to stabilize the samples for handling. Samples were then cut to thicknesses of between 0.2 and 0.8 mm on an oil-lubricated, low-speed saw in the X-Z and/or Y-Z planes of the strain ellipsoid (perpendicular to the planar fabric and parallel to any lineation or known fault slip direction). For convenience, both natural and laboratory samples were oriented in the XTG apparatus so that the shear sense was horizontal in the machine geometry and pole figure output, with either sinistral or dextral shear as indicated on the figures below.

4.2. Laboratory Shear Experiments

[19] Twenty-five laboratory experiments were performed on montmorillonite and montmorillonite-quartz mixtures using a servo-controlled, double-direct shear testing apparatus at room temperature and humidity [e.g., *Ikari et al.*, 2007]. In this configuration, two layers of gouge are sheared simultaneously while sandwiched between three forcing blocks. The side forcing blocks are held in place by applying a horizontal normal stress, which is maintained via servo-control, while the central block slides between the side blocks at a controlled displacement rate, inducing shear. Both the center and side blocks have roughened surfaces which consist of triangular grooves 0.8 mm deep that ensure slip within the gouge rather than along the boundary (see *Saffer and Marone* [2003] for detailed description of the experimental configuration). Gouge layers were prepared using a leveling jig to produce a uniform frictional contact area (5 × 5 cm) and initial thickness (4 mm). Layers were compacted to 2–3 mm under normal load prior to shearing.

[20] Our synthetic gouge layers consisted of commercially available high-purity Ca-montmorillonite powder (GSA Resources Inc.) and pure quartz sand (F110, U.S. Silica Co.). X-ray diffraction and SEM analysis of the montmorillonite indicates that it is a dioctahedral smectite (Ca-montmorillonite *sensu strictu*), which contains two partially filled water interlayers at room humidity and which expands to two full interlayers when solvated with ethelyne glycol. The montmorillonite has a mean grain size of 60 μm with 80% of the grains between 3 and 142 μm and contains trace amounts of heulandite and quartz (<1%) [*Ikari et al.*, 2007]. The quartz powder has subangular grains that range in size from 50 to 250 μm with a mean grain size of 127 μm and is >99% pure.

[21] Synthetic gouge samples were tested at applied normal stresses ranging from 10 to 150 MPa, for a series of gouge compositions ranging from 0 to 90 weight % quartz. In several of the experiments, normal stress was increased in steps; typical normal stress histories within an individual shearing experiment were 5, 10, 15, and 20; 30, 40, 50, and 75; and 100, 125, and 150 MPa (e.g., Figure 3). Samples were sheared at sliding velocities from 1 to 300 μm/sec. Gouge layers were subject to shear strains ranging from 0 (simple compaction) to ~22, which was calculated by integrating the measured slip increments divided by the instantaneous layer thickness (Table 3). Load point displacement of the vertical loading ram, which applies shear load, was corrected for elastic stiffness of the apparatus to produce true shear displacement [e.g., *Mair and Marone*, 1999]. Because several of our experiments were conducted at multiple normal stresses, we used only the shear strain at the highest normal stress to compensate for the effect of strain history. A total of 69 XTG measurements were made from samples prepared from the friction experiments (Table 2).

4.3. XTG Measurement Procedure

[22] Natural and synthetic gouge fabric intensities were measured on a modified Enraf-Nonius CAD4 single crystal X-ray diffractometer in transmission mode using the method of *van der Pluijm et al.* [1994]. The machine uses a molybdenum source and has a beam diameter of ~1 mm. The natural samples were measured at 23 mA and 43 kV, and the experimental samples were run at 15 mA and 35 kV, because the peak intensities for the experimental materials (which are bimineralic or monomineralic and thus diffract much more intensely per unit volume than a polyphase mixture of equal volume) were too high to permit accurate fabric quantification at higher voltages. Repeat analysis of the same sample at both voltages yielded MRD's that were identical within 2–3%. Owing to the extremely friable nature of some natural gouges and most of the experimental gouges, samples were cut thicker than the 0.2 mm by *van der Pluijm et al.* [1994]. Multiple analyses on samples from competent material that were cut both at 0.2 mm and 1.0 mm thickness indicate that fabric intensity (as measured in MRD units, multiples of a random distribution) varied by less than 10% between these samples. This minor difference in fabric intensity indicates that the relatively thick samples used in this study do not significantly affect our fabric intensity measurements, or comparisons with prior work.

[23] XTG analysis for a gouge sample is a two-step process. First, we scan over the range 1–12° 2Θ Mo Kα (or 2–26° for 2Θ Cu Kα) to identify the (*hkl*) peaks of the clay phases in a sample. Second, we measure the intensity of the clay phase of interest (usually the (001) peak) at each of ~1300 different orientations to collect a pole figure. This provides a quantitative measure of phyllosilicate fabric intensity. The principal (*hkl*) peaks of clay minerals can be

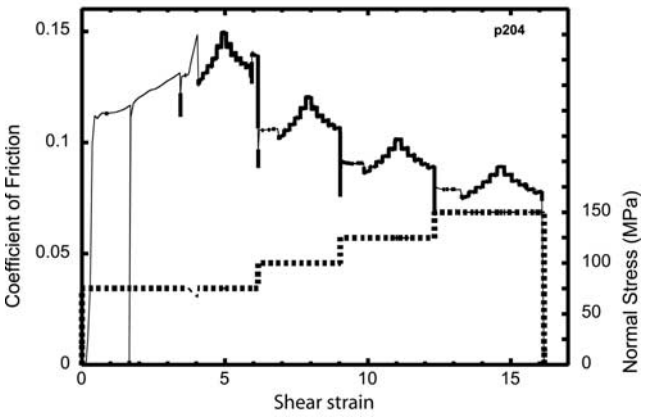

Figure 3. Plot of representative sliding friction test with stepped normal stress. Shown is a plot of normal stress versus shear strain (dotted line, right axis) superimposed over a plot of coefficient of sliding friction versus shear strain (solid line, left axis).

clearly distinguished on the Mo-source 2Θ pattern. Each sample is characterized using conventional XRD techniques [*Moore and Reynolds*, 1997] prior to XTG analysis to distinguish between peaks of clay phases (e.g., kaolinite (001) and chlorite (002)) that may be indistinguishable on the lower-resolution Mo-source 2Θ scan. Details of the full mineralogical characterization are given by Haines (unpublished thesis, 2008).

[24] The second step of the XTG analysis involves collecting the pole figure. The X-ray detector is first moved to the position that corresponds with the d spacing of the prominent peak of the clay phase of interest (e.g., 14 Å for smectite (001), 10 Å for illite (001), 9.8 Å for sepiolite (110), 10.5 Å for palygorskite (110) and 7 Å for both chlorite (002) and kaolinite (001)). The sample is then rotated both in its plane and about a vertical axis through a total of 1296 different orientations, measuring the peak intensity at each orientation with a count time of 2 s, covering roughly 65% of a full hemisphere. When the scan is complete, the pole figure of the diffracted beam is smoothed using a two-cycle smoothing process and contoured using multiples of a random distribution [MRD]. The pole figures are corrected for X-ray absorption and the extrapolation to a full pole using the procedures of *van der Pluijm et al.* [1994]. The fabric intensity we report is the maximum measured MRD value of the pole figure.

[25] Each gouge sample was scanned at a minimum of two locations on the cut face surface. A total of 87 pole figures from natural gouges were collected for this study from analyses of 37 XTG samples cut from 22 hand specimens collected from 9 faults. XTG measurements were carried out on the primary clay mineral as identified in each sample by the Mo 2Θ scan and XRD characterization. Where more than one clay phase was identified in a single sample, as at Badwater-1 and at Copper Canyon, separate measurements were made for each clay phase identified as listed in Table 2.

5. Results

5.1. Natural Fault Gouges

[26] Our fabric intensity data for natural faults show that clay-rich gouges have uniformly weak fabrics (Figure 4). Clay fabrics in the 22 natural gouge samples measured in this study have an average MRD of 2.5 with a standard deviation of 0.5. The minimum observed MRD was 1.7, and the maximum was 4.0 (Table 1). In all cases, fabric maxima as measured by XTG are subparallel to the crude foliation in many gouges visible at outcrop. Where a P foliation [e.g., *Logan et al.*, 1979] was visible at outcrop, the fabric intensity maxima as determined by XTG is subparallel to the visible P foliation and not to the "Y" or R surfaces. When a P foliation was not visible, fabric intensity maxima were subparallel to the fault zone margins. Most clay gouges that were visibly foliated had slightly higher fabric intensities (average = 2.8, $1\sigma = 0.5$) than those that were not visibly foliated (average = 2.3, $1\sigma = 0.5$). Sample anisotropy was minor, samples cut in the XZ plane of the strain ellipsoid had MRD's that average 0.1 greater than those cut in the YZ plane ($1\sigma = 0.34$, N = 15).

[27] Our results are consistent with previous findings [*Yan et al.*, 2001; *Solum et al.*, 2003, 2005, J. Solum et al., unpublished data, 2005; A. Schleicher et al., unpublished data, 2007]. When prior results are combined with our data to encompass gouges from a variety of tectonic environments and with a range of clay mineral compositions, the average fabric intensity distribution changes only slightly. The merged data sets (N = 142; this study N = 90, previous data N = 52) have an average MRD of 2.6 with a standard deviation of 0.6. The minimum observed MRD in a clay-rich fault gouge was 1.7 and the maximum was 4.0 (Figure 4). The uniformly weak fabrics observed from gouges in a total of 15 faults from a variety of tectonic environments indicate that this is a universal characteristic of clay-rich fault gouges.

[28] When the fault gouge fabric intensity data are separated by tectonic environment, such as thrust faults, low-angle normal faults and strike-slip faults, the fabric intensity distributions are essentially indistinguishable. Thrust faults have an average MRD of 2.6 ($1\sigma = 0.52$, N = 27), low-angle normal faults have an average MRD of 2.7 ($1\sigma = 0.52$, N = 90), and strike slip faults have an average MRD of 2.5. ($1\sigma = 0.44$, N = 24) (see Figure 4). High-angle normal faults have a similar average MRD of 2.4, although the data set is much smaller (N = 5, min = 1.79, max = 3.19). Minima and maxima are also are very similar for the three larger distributions; the minima of the three distributions are all 1.8, while the maxima range from 3.5 to 4.0. The agreement among fabric intensities for gouges from differing tectonic environments indicate that the clay fabric-forming process is essentially independent of the tectonic environment (Figure 4).

[29] The clay mineralogy of the gouge imparts little effect on the measured fabric intensity. When the gouge fabric intensity data from the combined XTG data sets are organized by clay mineral, a similar pattern emerges to that described above. Illitic and chloritic gouges have essentially identical fabric intensities, 2.6 for illite ($1\sigma = 0.49$, N = 57) and 2.5 for chlorite ($1\sigma = 0.47$, N = 52). Sepiolite and palygorskite (both are phyllosilicates with a fibrous morphology as opposed to the platy morphology typical of most clay minerals) and corrensite-dominated gouges also have very similar average fabric intensities: 2.8 for sepiolite and palygorskite ($1\sigma = 0.51$, N = 20) and 2.6 for corrensite ($1\sigma = 0.65$, N = 9). Gouges where more than one clay phase was measured commonly have very similar fabric intensities for both phases. The fabric intensities for illite from fault gouge are,

Table 2. Fabric Intensity Measurements for Natural Faults Sampled in This Study

				Fabric Strength (MRD)			
Outcrop	Field Sample	Sample Chip	Clay Mineral	Measurement 1	Measurement 2	Measurement 3	Measurement 4
			Ruby Mountains, Nevada				
Clover Hill	Clover-1	CLO 1b	Kaolinite	1.96	1.79		
	Clover-2	CLO 2a	Illite	2.38	2.42		
Secret Pass	Secret Pass 4-1	Sec 4-1 (1)	Illite	2.57	2.70		
		SEC 4-1 (2)	Illite	2.93	2.78		
	Secret Pass 4-3	SEC 4-3 (1)	Smectite	1.77	1.89		
		SEC 4-3 (2)	Smectite	1.75	1.74		
	Secret Pass 4-5	SEC 4-5 (3)	Illite	1.92	2.00		
	Secret Pass 4-6	SEC 4-6 (3)	Illite	2.51	2.50		
		SEC 4-6 (5)	Illite	2.12	1.80		
			Death Valley, California				
Badwater-1	Badwater 1-1	Bad 1-1 (1)	Illite	2.65			
		Bad 1-1 (1)	Chlorite	2.05	1.90		
		Bad 1-1 (2)	Chlorite	2.41	2.15		
	Badwater 1-2	Bad 2-1 (1)	Illite	2.38	2.54		
		Bad 2-1 (2)	Illite	2.50	2.03		
	Badwater 1-4	Bad-4a	Illite	2.75	2.49		
Copper Canyon	Copper Canyon-1	Cop-1a	Chlorite	3.06	3.02	3.17	
		Cop-1a	Corrensite	2.74	3.92	3.22	
		Cop-1b	Chlorite	2.16	3.28	3.67	
		Cop-1b	Corrensite	2.2	2.97		
		Cop-1b	Illite	3.23			
Dante's View	Dante-1	Dante-1	Palygorskite	2.32	2.45	2.18	
Exclamation Rock	Exclamation Rock W-1	! RockW-1 (1)	Illite	3.62	3.39		
		! Rock W-1 (2)	Illite	3.56	3.00		
	Exclamation Rock W-2	! Rock W-2 (1)	Illite	4.01	2.41		
		! Rock W-2 (1)	Chlorite	2.04			
Size 36 canyon	Size 36 Upper	36U (1)	Illite	2.30	2.36		
		36U (2)	Illite	2.40	3.25		
	Size 36 Lower	36L-1 (1)	Illite	2.38	2.27		
		36L-1 (2)	Illite	2.49	3.16		
	Size 36 FW breccia	36bx-1 (1)	Illite	2.30			
		36bx-1 (2)	Illite	2.22	2.41		
Mormon Point-2	Mormon-2	Mor-2 (1)	Chlorite	2.41	2.44		
		Mor-2 (2)	Chlorite	1.99	2.24		
Mormon Point -3	Mormon 3-1-1	MP31 1-1(1)	Sepiolite	2.8	3.15		
		MP31 1-1(2)	Sepiolite	2.75	3.63		
		MP31 1-2	Sepiolite	3.26	3.71		
	Mormon 3-1-2	MP3-1 2-1 (1)	Sepiolite	2.58	1.94	2.36	
		MP3-1 2-1 (1)	Smectite	2.61			
		MP31 2-2	Sepiolite	3.09	2.49	1.92	2.44
	Mormon 3-1 (G)	MP31 G(1)	Chlorite	2.02	2.27		
		MP31 G1(2)	Chlorite	2.41	2.35		
			Salton Sea Detachment, California				
Salton Sea "571"	Salton 571	571-1	Smectite	2.69	2.99		
			Peramola Thrust, NE Spain				
Peramola thrust	Peramola-1	PER-1a	Corrensite	1.83	2.14		
		PER-1b	Corrensite	2.47	2.20		

however, considerably weaker than those observed in illite-dominated shales, where the observed MRD's typically range from 3.0 to 6.0. Smectite and kaolinite fabric intensities for fault gouges are somewhat weaker than those for gouges that are dominated by other clay minerals; MRD's for gouges dominated by smectite and kaolinite average 2.2 for smectite (min = 1.7, max = 3.0, N = 6) and 1.9 for kaolinite (min = 1.8, max = 2.0, N = 2).

5.2. Spatial Distribution of Clay Fabric Intensity in Low-Angle Normal Fault Gouges

[30] To examine intrafault variations in clay fabric intensity and to test the strain localization proposal of *Cowan et al.* [2003], we measured clay fabric intensity along a transect across two low-angle normal faults (the Gregory Peak detachment at Size 36 Canyon and the Badwater Detachment). Three samples from each detachment were analyzed, one from the principal slip plane (PSP), one from the central region of the clay gouge layer and one from the footwall breccia (Figure 5). A total of 11 fabric measurements were made from the 3 samples at each outcrop. At Size 36 Canyon, a clear shear fabric is preserved, and the clay fabric measurements from the lower gouge and the footwall are both subparallel to the macroscopic P foliation. The fabric from the PSP is subparallel to the PSP, which is a Y surface (Figure 5). Fabric intensity increases only slightly from the footwall breccia toward the PSP. The footwall breccia MRD's averaged 2.3 (min 2.2, max 2.3, N = 3), while the lower and the PSP fabric intensities each averaged 2.6, (min 2.3, max 3.2, N = 4). At the Badwater outcrop, which

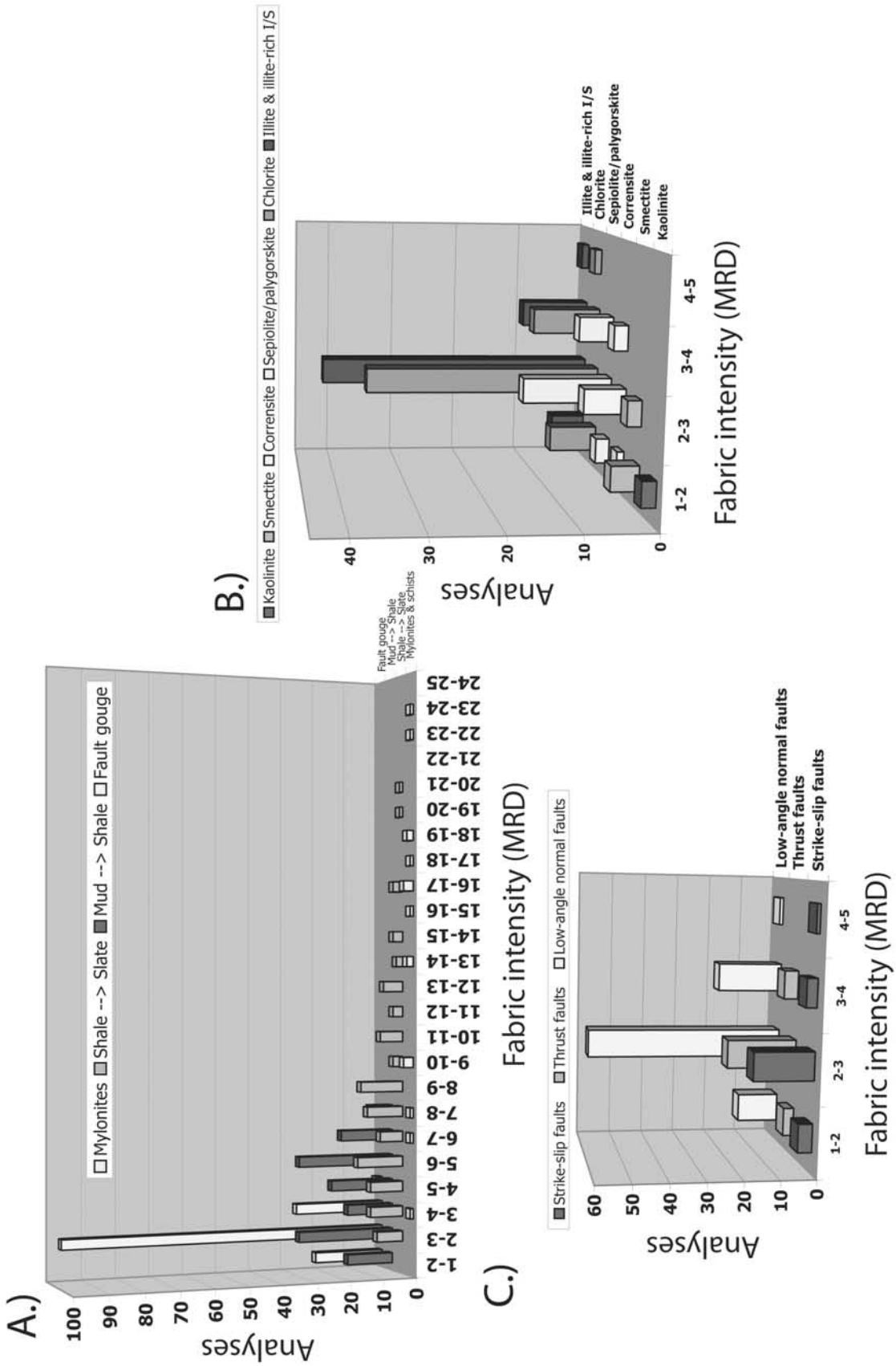

Figure 4. Natural clay fabric intensity data. (a) Phyllosilicate fabric intensities measured from various geologic environments. (b) Fabric intensites of fault gouges separated by predominant clay mineralogy of gouge. (c) Fabric intensity of fault gouges from various tectonic environments. Data from *Tullis and Wood* [1975], *Lipshie et al.* [1976], *O'Brien et al.* [1987], *Sintubin* [1994a, 1994b], *Ho et al.* [1995, 1996, 2000], *Jacob et al.* [2000], *Yan et al.* [2001], *Solum et al.* [2003, 2005], J. Solum et al. (unpublished data, 2005), *Aplin et al.* [2006], *Day-Stirrat et al.* [2008], A. Schleicher et al. (unpublished data, 2007), and this study.

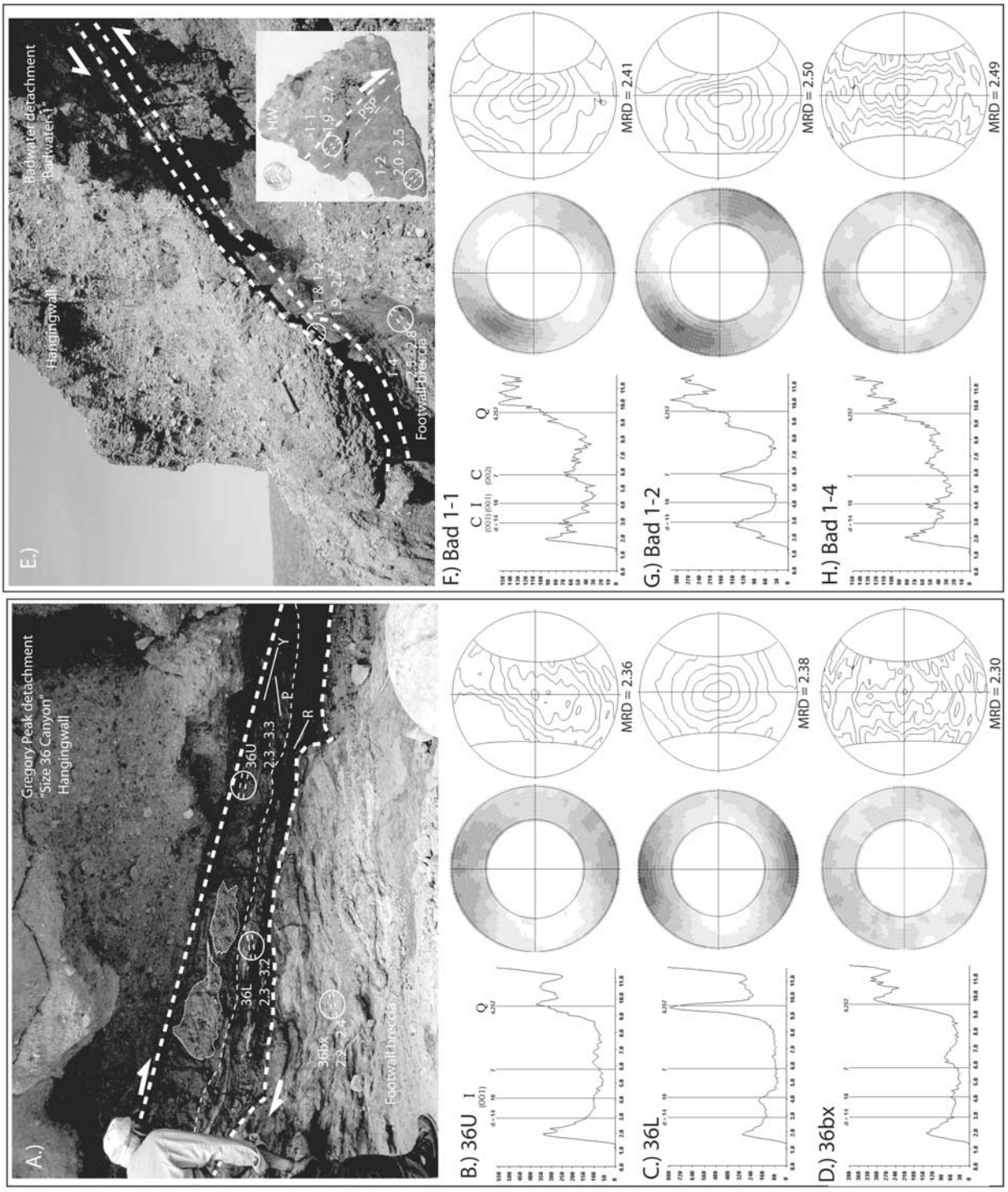
A.)
Gregory Peak detachment
"Size 36 Canyon"
Hanging wall
36U
36L
36bx
2.3 - 3.3
2.3 - 3.2
2.3 - 2.4
Y
P
R
Footwall breccia
B.) 36U
C.) 36L
D.) 36bx
MRD = 2.36
MRD = 2.38
MRD = 2.30
E.)
Hanging wall
Radwater detachment
"Badwater-1"
1-1
1.9 - 2.7
P3p
1-2
2.0 - 2.5
1-1 & -2
1.9 - 2.7
1-4
2.8
Footwall breccia
HW
F.) Bad 1-1
G.) Bad 1-2
H.) Bad 1-4
MRD = 2.41
MRD = 2.50
MRD = 2.49

Figure 5

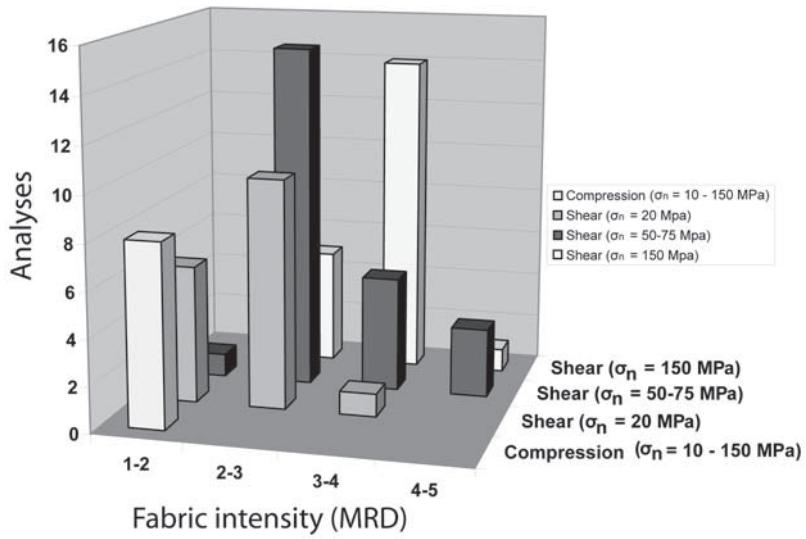

Figure 6. Summary of experimental clay fabric intensity measurements. Shown are data from all experiments and binned by final normal stress.

lacks a strong shear fabric; the gouge zone foliation is only barely visible to the naked eye. Measured fabric intensity maxima are subparallel to the weak fault-parallel foliation visible at outcrop (Figure 5). The fabric intensity decreases slightly with proximity to the PSP. The footwall breccia had MRD's of 2.5 and 2.8, while the lower gouge averaged 2.4 (min = 2.0, max = 2.5, N = 4) and the PSP averaged 2.2 (min = 1.9, max = 2.7, N = 5).

5.3. Synthetic Gouges

[31] The gouges formed under laboratory conditions exhibit similarly weak fabric intensities (MRD 1.7–4.6) to the natural samples (Table 3 and Figure 6). The clay fabric intensities from the 100% montmorillonite samples, which were compressed but not sheared (pure compaction, experiments P233, P234 and P1314), are very weak, and pole figures indicate maxima that are parallel with the applied normal stress. Measured MRD's average 1.7, with a standard deviation of 0.1, and vary only slightly, with a minimum of 1.6 and a maximum of 1.8. The MRD values for the samples with zero shear strain do not vary systematically with normal stress; fabric intensities for samples compressed at 10, 50, and at 150 MPa are effectively identical and uniformly weak. The fabric intensity maxima in these samples are parallel to the applied normal stress, which indicates that the clay crystallites are aligning, albeit very weakly, perpendicular to the compressive stress (Figures 7 and 8). We note that fabric intensity does not increase noticeably with increasing normal stress beyond 10 MPa. This observation has important implications for the March strain model, which will be discussed below.

[32] Samples that are both compressed and sheared, exhibit substantially stronger fabrics compared to those that were only compressed. The MRD values of sheared samples average 2.9, and ranging from 1.7 to 4.6 (Figure 7). Fabric intensity increases with increasing shear strain at shear strains from 0 to ~20. The data indicate that fabric evolves nonlinearly with strain; most of the increase in intensity occurs between shear strains of 0 and 5. Unlike samples that were compressed without shear, sheared samples (Figure 7) exhibit fabric maxima that align at an angle both oblique to the maximum compressive stress and to the shear direction, and subparallel to the P shear orientation of *Logan et al.* [1979].

[33] The orientation of clay fabrics in the experimental samples is analogous to both our observations and prior work on clay foliation in natural fault zones [*Chester et al.*, 1985; *Cladouhos*, 1999b; *Cowan et al.*, 2003; *Hayman*, 2006]. The degree of rotation of the maxima from normal stress parallel toward the applied shear stress in the experimental samples increases with increasing strain, ranging from ~0° at 0 shear strain, to a maximum of 30–45° at shear strains of ~6 (Figure 8). Maxima for samples with a shear strain of 0, i.e., simple compression, are all parallel to the applied normal stress. The samples with a shear strain of 0.5 exhibit either

Figure 5. Spatial variations in clay fabric intensity across low-angle normal faults. (a) Field photo of outcrop at Size 36 Canyon showing sample locations (circles). Dashed lines inside circles indicate orientation of measured clay fabric at each location. MRD range for each sample is shown below sample number. (b–d) Data output from samples 36U, 36L, and 36bx. Figure 5b shows raw Mo-source XRD pattern with markers indicating position of peaks for prominent phases (I, illite; C, chlorite; Q, quartz). Figure 5c shows raw pole figure oriented relative to the outcrop indicating fabric orientation at outcrop. Figure 5d shows contoured pole figure centered to demonstrate peak intensity was measured. (e) Field photo of outcrop at Badwater-1. Inset photo shows sample of gouge from uppermost gouge and PSP taken at upper circle in main photo. Circles in inset show location of material for samples 1-1 and 1-2. Dashed lines inside circles indicate orientation of measured clay fabric at each location. MRD range for each sample is shown below sample number. (f–h) Data output from samples Bad 1-1, Bad 1-2, and Bad 1-4. Layout is same as in Figures 5b–5d.

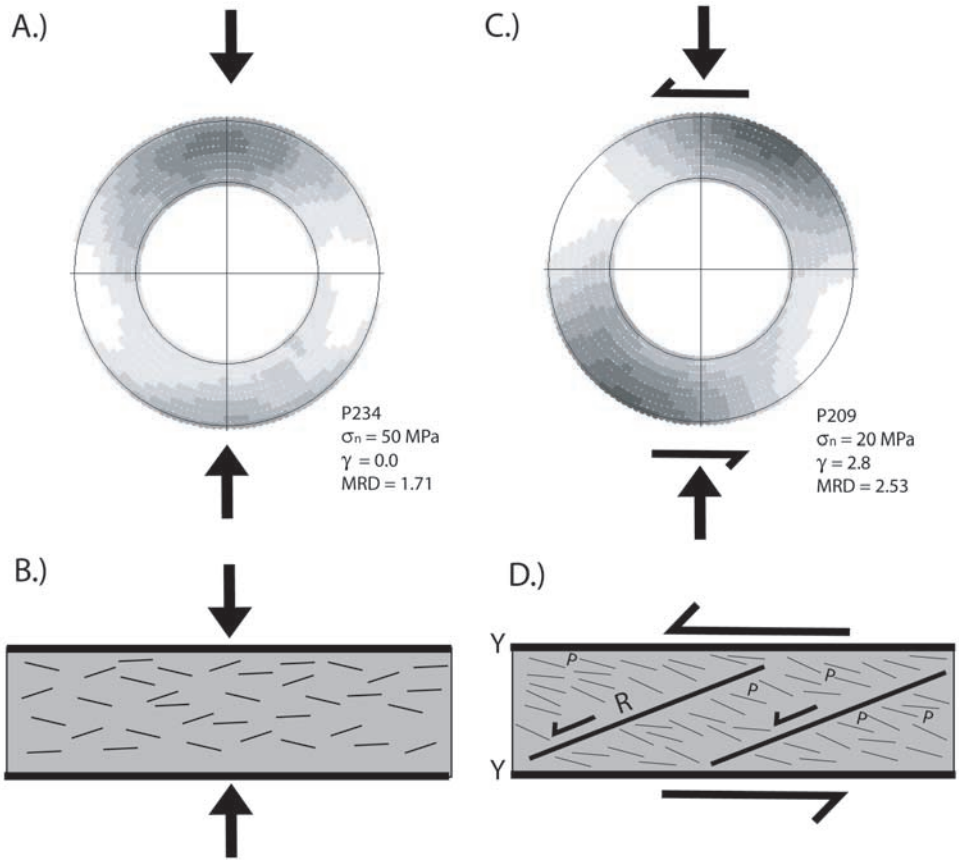

Figure 7. Representative pole figures from experimental samples subjected to compression versus compression and shear illustrating relative effects on clay fabric. (a) Pole figure from experiment P234 (100% montmorillonite). Compression was vertical. Darker shading indicates greater density of X-ray counts. (b) Schematic representation of clay fabric in Figure 7a. (c) Pole figure from experiment P209 (50% montmorillonite). Compression was vertical and sense of shear was top to the left. (d) Schematic representation of clay fabric in Figure 7c.

slightly inclined maxima or multiple maxima that are irregular and rotated at low angles (5–15°), both toward and away from the applied shear stress Where two maxima occur, they are both within 10° of the applied normal stress, and may represent a transition from a compression-dominated fabric to a shear-dominated fabric. Maxima for the samples with a shear strain of ~3 are rotated 20–35° toward the applied shear stress while the maxima for samples with a shear strain of ~20 are rotated 30–45° toward the applied shear stress (Figure 8).

[34] SEM images further document fabric evolution with increasing strain (Figure 9). The samples subjected to compression only exhibit no visible fabric, consistent with MRD's of 1.6 to 1.8. These fabrics are only slightly more coherent than expected for a random distribution of clay grains. Samples that are compressed and sheared, are characterized by boundary parallel Y surfaces at the sample margins and clearly developed R shears with polished and striated surfaces (Figure 9). The sheared samples also have a crude P foliation, although, interestingly, the P foliation in the samples is at a lower angle relative to the sample margins (typically 5°), compared to the primary orientation of the phyllosilicate crystallites determined from XTG analysis, which is 25–30° from the sample margin.

[35] Clay fabric intensity in the experimentally deformed 100% montmorillonite samples increases systematically with increasing shear strain and normal stress (Figure 10). Under pure compaction, fabric intensity does not increase with increasing normal stress, whereas when both normal stress and shear stress are applied, normal stress controls the fabric intensity achieved at a given strain and also the amount of strain required to acquire a given fabric intensity (Figure 10). Samples subjected to compression but not shear exhibit MRD's from 1.6 to 1.8, whereas samples that were subjected to shear strains of ~20 exhibited MRD's of 3.4 to 4.6. Samples compressed at 10–25 MPa acquired a weak fabric at strains up to ~3 and maintained that fabric intensity up to a strain of 21; MRD's range from 1.7 (no fabric) to a maximum of 2.5, with most samples having an MRD of 2.1 to 2.4. Samples that were compressed at a maximum normal stress of 50–75 MPa and sheared to a shear strain of ~22 have MRD's that range from 2.3 to 4.3, with fabric intensity increasing with increasing strain from an average MRD of 2.6 at a strain of ~4, to an average MRD of 3.5 at a strain of 22.5. Samples that were compressed at a maximum normal stress of 150 MPa have MRD's from 2.2 to 4.0, with fabric intensity increasing systematically from an average intensity of 2.2 at a strain of 0.5 to an average fabric intensity of 4.0 at a shear strain of 20.5.

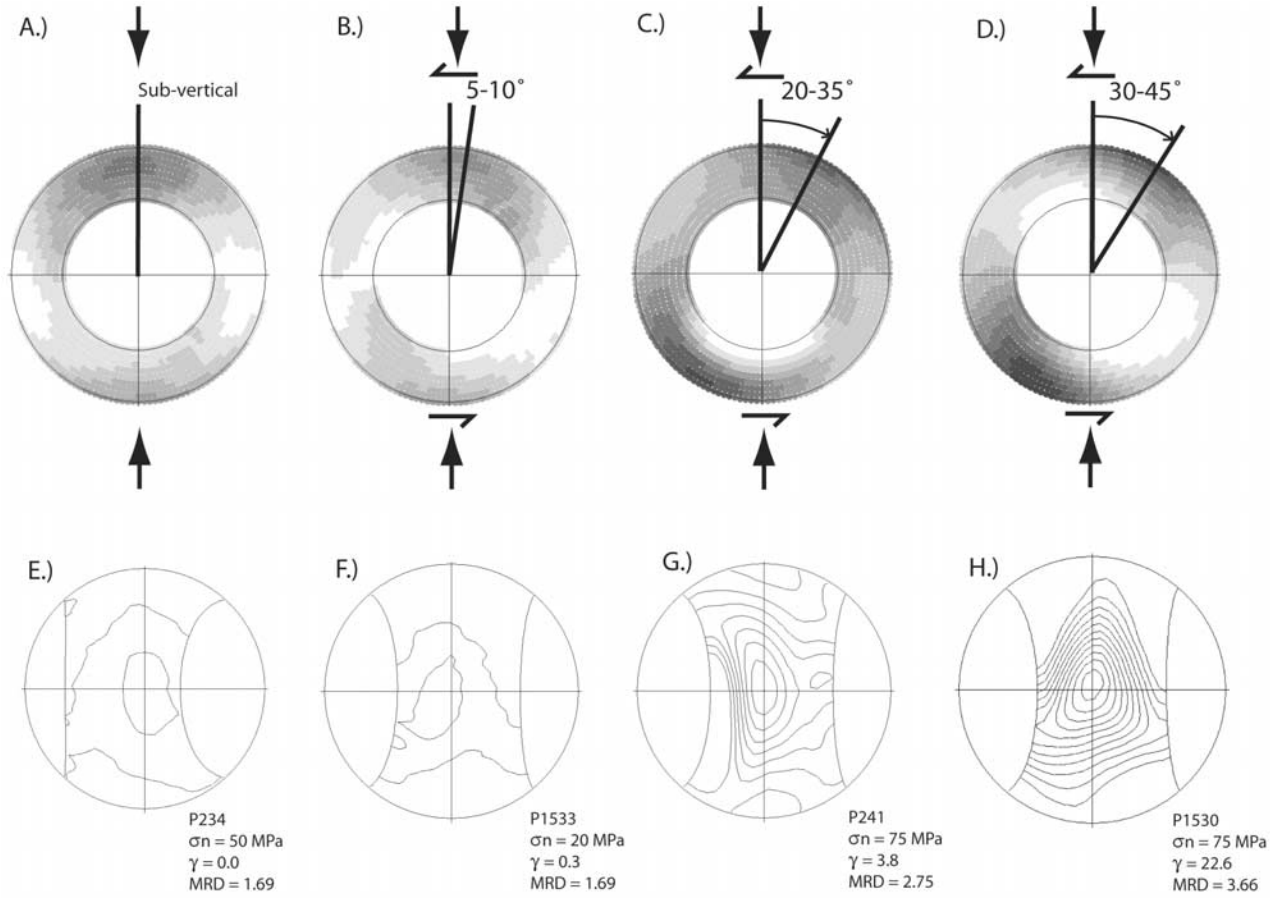

Figure 8. XTG pole figures of experimental gouges showing effect of increasing shear strain on clay fabric orientation and intensity for Experiment (a) P234 (100% montmorillonite, σ_n = 50 MPa, γ = 0.0), (b) P1533 (100% montmorillonite, σ_n = 20 MPa, γ = 0.3), (c) P241 (100% montmorillonite, σ_n = 75 MPa, γ = 3.8), and (d) 1530 (100% montmorillonite, σ_n = 75 MPa, γ = 22.6). Range of angles indicated is the range of rotations of intensity maxima from vertical observed from samples with a given shear strain. Note gradual rotation of the maxima from σ_1 with increasing shear strain, along with some increase of fabric intensity with increasing strain at strains >3. (e–h) Rotated pole figures from Figure 8a–8d, respectively. Centering of contour lines demonstrate fabric intensity maxima were measured; contour interval is 0.25 MRD.

[36] At all normal stresses, the maximum fabric intensity is typically reached within a shear strain of ~5, with little to no further fabric intensification with subsequent shear strain. This is consistent with the results of *Saffer and Marone* [2003], which show evolution of the frictional strength over the same range of shear strain. Our data suggest that at shear strains >5, strain is accommodated primarily along shear surfaces and that the spectator regions are acting to "preserve" fabrics acquired earlier in the strain history of the material. The clay content of our synthetic samples has almost no resolvable effect on the phyllosilicate fabric intensity (Figure 11). The MRD values for clay-rich and clay-poor material are essentially identical for a given normal stress and shear strain.

6. Discussion

6.1. Clay Fabric in Natural Gouges

[37] Three key points emerge from our fabric intensity measurements of natural fault gouge. First, natural fault gouges have uniformly weak fabrics when compared to the fabrics of phyllosilicate-rich rocks in other geologic environments. Fault gouge fabric intensities range from a low of about 1.7 to a maximum of about 4.0, with an average of 2.6. These fabric intensities are low compared to those measured from rocks formed in other geologic environments, Previously published XTG data show that, for rock in the mud-to-shale transition, MRDs range up to ~7 [*Sintubin*, 1994b; *Ho et al.*, 1999; *Aplin et al.*, 2006; *Day-Stirrat et al.*, 2008] whereas, for rocks in the shale-to-slate transformation, MRDs range up to ~20 [*Tullis and Wood*, 1975; *Sintubin*, 1994a; *Ho et al.*, 1996, 2001; *Jacob et al.*, 2000]. For comparison, mylonites and schists have MRDs ranging from ~4 to as high as 24 [*Lipshie et al.*, 1976; *O'Brien et al.*, 1987] (Figure 4).

[38] A second key result is that tectonic environment does not significantly impact clay fabric development in fault zones. Thrust faults, strike-slip faults and both low-angle and high-angle normal faults all have similar fabric intensities. The third key result is that clay mineralogy of a natural

Table 3. Stress/Strain Histories and XTG Measurements of Experimental Samples[a]

Experiment	% montmorillonite	σ_n (MPa)	Sliding Velocity (mm/s)	Shear Strain at End σn 1	Shear Strain at End σn 2	Shear Strain at End σn 3	Shear Strain at End σn 4	Final Shear Strain	Final σn (MPa)	Shear Strain During Final σn	MRD					
											Measurement 1	Measurement 2	Measurement 3	Measurement 4	Measurement 5	Measurement 6
P203	90	20, 30, 40, 50	Stepped- 1, 3, 10, 30, 100, 300	7.4	11.2	15.9	21.5	21.4	50	5.5	3.66	4.55	3.39	3.49		
P204	90	75, 100, 125, 150	Stepped- 1, 3, 10, 30, 100, 300	6.2	9.0	12.4	16.1	16.1	150	3.8	3.71	3.85	3.82	3.44	3.08	3.04
P205	70	5, 10, 15, 20	Stepped- 1, 3, 10, 30, 100, 300	4.4	6.6	9.4	12.6	12.5	20	3.2	2.19	1.72				
P209	50	5, 10, 15, 20	Stepped- 1, 3, 10, 30, 100, 300	3.7	5.7	8.0	10.8	10.8	20	2.8	3.24	2.53	2.27			
P211	50	30, 40, 50, 75	Stepped- 1, 3, 10, 30, 100, 300	4.3	6.4	8.9	12.0	12.0	75	3.1	2.72	2.79				
P212	50	100, 125, 150	Stepped- 1, 3, 10, 30, 100, 300	4.6	6.9	9.9		9.9	150	2.9	2.98	3.25				
P213	30	5, 10, 15, 20	Stepped- 1, 3, 10, 30, 100, 300	3.5	5.3	7.5	10.0	10.1	20	2.5	1.94					
P215	30	30, 40, 50, 75	Stepped- 1, 3, 10, 30, 100, 300	4.2	6.4	8.9	12.0	12.0	75	3.1	2.41	2.18				
P216	30	100, 125, 150	Stepped- 1, 3, 10, 30, 100, 300	4.2	6.3	8.9		8.9	150	2.6	2.30	2.18				
P220	10	30, 40, 50, 75	Stepped- 1, 3, 10, 30, 100, 300	3.7	6.1	8.2	11.1	11.1	75	2.9	2.59	2.22				
P221	10	100, 125, 150	Stepped- 1, 3, 10, 30, 100, 300	4.1	6.1	8.9		8.6	150	2.8	3.65	3.84				
P229	100	5, 10, 15, 20	Stepped- 1, 3, 10, 30, 100, 300	4.1	6.3	9.0	12.3	12.3	20	3.3	1.95	2.00	2.41			
P233	100	10	No displacement	0.0				0.0	10	0.0	1.80	1.63				
P234	100	50	No displacement	0.0				0.0	50	0.0	1.69	1.62	1.84	1.71		
P241	100	30, 40, 50, 75	Stepped- 1, 3, 10, 30, 100, 300	5.3	7.9	11.1	14.8	14.8	75	3.8	2.75	2.49	2.80	2.36	2.66	
P1313	100	100, 125, 150	10	6.0				6.0	150	6.0	3.64	3.71				
P1314	100	150	No displacement	0.0				0.0	150	0.0	1.70	1.69				
P1315	100	150	10	0.5				0.5	150	0.5	2.32	2.48				
P1528	100	150	10	20.5				20.5	150	20.5	3.86	4.38	3.83	3.82		
P1529	100	75	10	7.2				7.2	75	7.2	4.10	2.98	2.59	2.46		
P1530	100	75	10	22.6				22.6	75	22.6	2.99	3.66	4.36	3.25		

Table 3. (continued)

Experiment	% montmorillonite	σ_n (MPa)	Sliding Velocity (mm/s)	Shear Strain at End σn 1	Shear Strain at End σn 2	Shear Strain at End σn 3	Shear Strain at End σn 4	Final Shear Strain	Final σn (MPa)	Shear Strain During Final σn	MRD Measurement 1	MRD Measurement 2	MRD Measurement 3	MRD Measurement 4	MRD Measurement 5	MRD Measurement 6
P1531	100	20	10	11.9				11.9	20	11.9	2.54	2.23	2.28			
P1532	100	20	10	0.3				0.3	20	0.3	1.77	2.00				
P1533	100	75	10	0.3				0.3	75	0.3	1.69					
P1551	100	20	10	21.3				21.3	20	21.3	2.36	2.43	2.33			

[a]Fabric intensity measured in multiples of random distribution units (MRD).

gouge has only a very minor effect on fabric intensity. Fabrics from chlorite-dominated clay gouges have similar intensities to clay gouges dominated by illite or illite-rich illite-smectite (>75% I in I/S). Gouges dominated by corrensite or sepiolite have similarly weak fabrics compared to those dominated by chlorite or illite, although there are fewer data than from gouges with the former mineral assemblages. Natural gouges dominated by smectite and kaolinite have slightly weaker fabrics that may result from postfaulting growth of the clay phases or the wavy morphology of smectitic clay phases.

[39] We suggest two possible explanations for the lower observed fabric intensities in smectitic-rich and kaolinite-rich clay gouges relative to chloritie-rich and illite-rich gouges. First, the data for smectite and kaolinite are derived from measurements on clay gouges from three ''low-angle'' normal faults, two of which (Clover Hill and Secret Pass) have ambiguous field evidence that smectite-rich and kaolinite-rich horizons in the gouge zone were present at the time of faulting. Thus, the very weak fabrics could have evolved as a result of clays that grew after fault slip ceased. If the fault surface was tectonically exhumed to higher levels in the crust, to a depth where differential stresses were lower, perhaps this led to a more isotropic clay fabric. Second, TEM images of smectite consistently show a distinctive wavy and irregular habit visible at very high magnifications [e.g., *Schleicher et al.*, 2006], whereas illite and chlorite at the same high magnifications typically have more planar morphologies. It is likely that the lower measured fabric intensities for smectite are at least partly a function of the differing crystallite morphology of smectite, although more study is required to validate this hypothesis.

[40] The observation that clay content in synthetic sheared samples has a small effect on fabric is in contrast with findings from sedimentary basins where the fabric intensity decreases systematically with increasing quartz content [*Curtis et al.*, 1980; *Sintubin*, 1994a, 1994b]. Two possible explanations exist. First, the MRD values observed in experimental gouges are so low that the effect of varying clay content is below measurement resolution. A similar comment can be made about the natural fault gouges, which also show low MRD values (Figure 4). For natural and laboratory gouge zones, a systematic difference of fabric intensity with nonclay mineral content may be unresolvable within the limitations of the XTG technique. A second possibility is that fabrics in sedimentary rocks are dominated by authigenic clay that grows during burial and diagenesis, with a smaller contribution from detrital grains that rotate by physical processes. In sedimentary basins, the growth of authigenic phases at and below the smectite-to-illite transition can produce abrupt increases in fabric intensity with depth [e.g., *Ho et al.*, 1996; *Day-Stirrat et al.*, 2008]. In these situations, it is possible that the presence of quartz or other nonplaty particles hampers authigenic clay growth. Our laboratory experiments do not involve authigenic grain growth and thus rotation of clay grains is the only process for fabric development. However, authigenic grain growth does occur in natural fault zones [e.g., *van der Pluijm et al.*, 2001]. In fault zones, if the preferred orientation of clay platelets is kept sufficiently weak by shearing, then the presence or absence of nonplaty particles, and whether they are detrital or authigenic in origin may not have a significant effect.

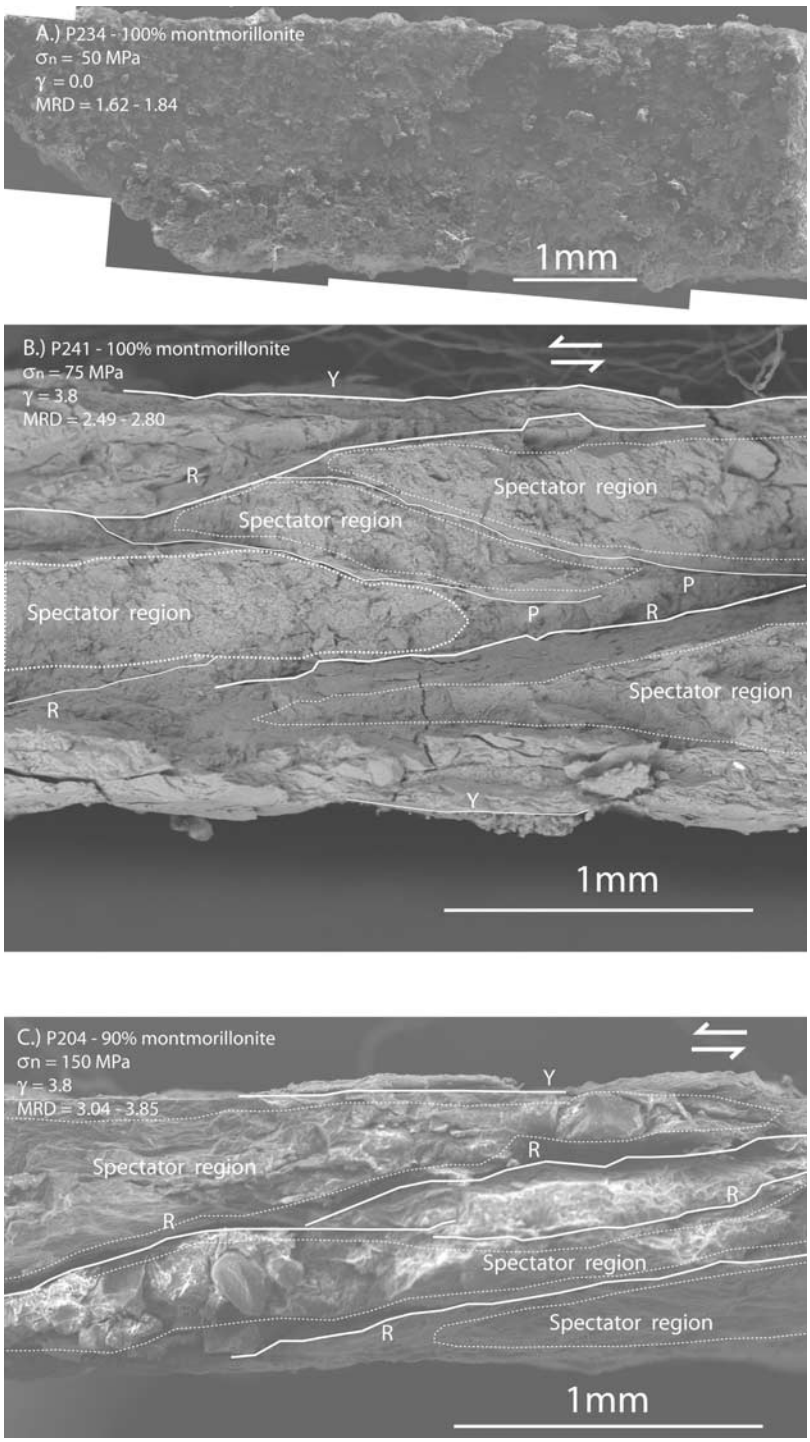

Figure 9. Annotated scanning electron images of experimental samples used in this study. (a) Photomosaic of SE images of sample P234, compressed at 50 MPa with no shear strain. Note the lack of a visible fabric. (b) SE image of sample P241, compressed at a maximum of 75 MPa and sheared during its final normal stress step to a strain of 3.8. Note the development of a clay fabric; R, Y, and P surfaces; and spectator regions. (c) SE image of sample P204, sheared at a maximum normal stress of 150 MPa and sheared during its final normal stress step to a shear strain of 3.8.

6.1.1. Implications of Natural Clay Fabrics for Permeability Anisotropy and Pore Pressure Retention

[41] Elevated fluid pressure localized within fault zones has been invoked as one possible mechanism explaining the apparent weakness of upper crustal faults [e.g., *Rice*, 1992; *Faulkner and Rutter*, 2001]. This weakening mechanism generally requires that fault zone permeability is sufficiently low, and possibly anisotropic, such that fluids cannot escape into the surrounding wall rock. Permeability anisotropy is especially important for models that invoke a lower crustal

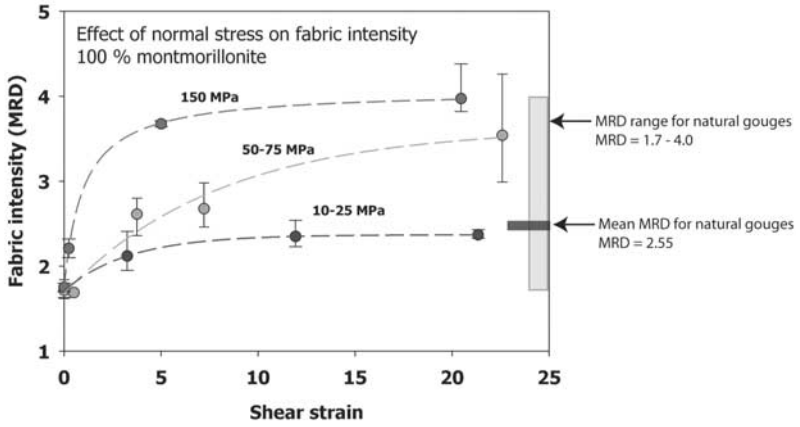

Figure 10. Plot of fabric data from experimental samples against shear strain for 100% montmorillonite samples. Shown are the average fabric intensity (circles), minimum and maximum fabric intensity measurements (vertical bars) for a particular friction experiment to highlight the role of shear strain in increasing fabric intensity at low shear strains, and of normal stress controlling the fabric intensity at high shear strains. Ranges for natural data are shown on the right-hand side for comparison.

or mantle source of fluids entering the fault zone at its base [e.g., *Rice*, 1992]. Our finding that fault gouge clay fabrics are weak, although they do form subparallel to macroscopic fault zone foliations, suggests that fabric anisotropy is unlikely to be large enough to effectively confine fluids. This conclusion is supported by our finding of negligible changes in fabric intensity between samples cut in the XZ and YZ planes of the strain ellipsoid. Moreover, the conclusion is supported by the findings of *Solum et al.* [2005] and *Hayman* [2006], as well as with recent studies that document little permeability anisotropy in clay-rich mudstones [*Yang and Aplin*, 2007]. Although permeabilities in clay-rich gouges are often low (10^{-16}–10^{-21} m^2 [e.g., *Morrow et al.*, 1984; *Gibson*, 1998; *Zhang and Cox*, 2000; *Crawford et al.*, 2002; *Davatzes et al.*, 2005], our clay fabric intensity measurements suggest that anisotropy may be weak. Thus, while low permeability may sustain high fluid pressures in clay-rich fault cores, anisotropy of permeability caused by strong phyllosilicate fabrics may not be a key control on the development or maintenance of locally elevated fluid pressures within faults.

[42] Macroscopic fabric elements common to many clay-rich gouges would also act against maintaining high fluid pressures in fault cores for long periods of time. The presence of P and R surfaces with significant lateral continuity observed in many clay gouges [e.g., *Cladouhos*, 1999a, 1999b; *Cowan*, 1999; *Cowan et al.*, 2003; *Hayman*, 2006] (Figure 5) would create conduits for fluid flow, which would act to reduce the capacity of the fault core to sustain high fluid pressures relative to the wall rock. Many low-angle normal faults have hanging walls that consist of loosely consolidated gravels and conglomerates (e.g., Figure 5). These hanging wall lithologies have visible primary porosity in the field which makes it unlikely that they will trap high fluid pressures in the adjacent gouge zones if the strain localization structures (“P”, R, and Y surfaces) in the gouge act as permeable pathways. It is thus probable that low-angle normal fault cores do not experience abnormally high fluid pressures relative to wallrocks unless the absolute gouge permeability is extremely low.

6.1.2. Natural Clay Fabrics and Shear Strain

[43] Our data from transects across low-angle normal faults approaching the principal shear plane (PSP) of *Cowan et al.* [2003] do not indicate a systematic increase in fabric intensity approaching the PSP. The probable explanation is that clay fabric intensity does not continuously increase with increasing shear strain, allowing for the larger shear strains posited near the PSP to accumulate without affecting the fabric intensity. This explanation requires that above some critical value for shear strain, clay fabric intensity remains essentially constant to allow very large shear strains to accumulate without developing strong fabrics, which is also suggested by our experimental work (see below). Another explanation is that the shear strain gradient across the detachment is more uniform than predicted by the conceptual model of *Cowan et al.* [2003]. The majority of outcrop exposures of low-angle normal faults show a general reduction in clast size approaching the PSP, but occasional clast to boulder size can be found within a few cm of the PSP (e.g.,

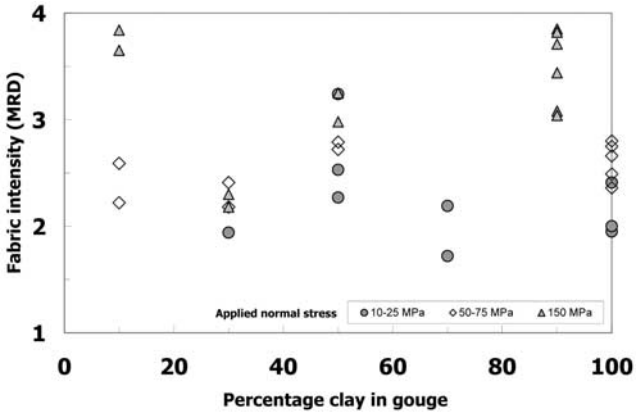

Figure 11. Graph showing the relationship of clay mineral content with fabric intensity for samples with shear strains of 2.5–3.5. Key shows applied normal stresses for final shear strain step for each experiment.

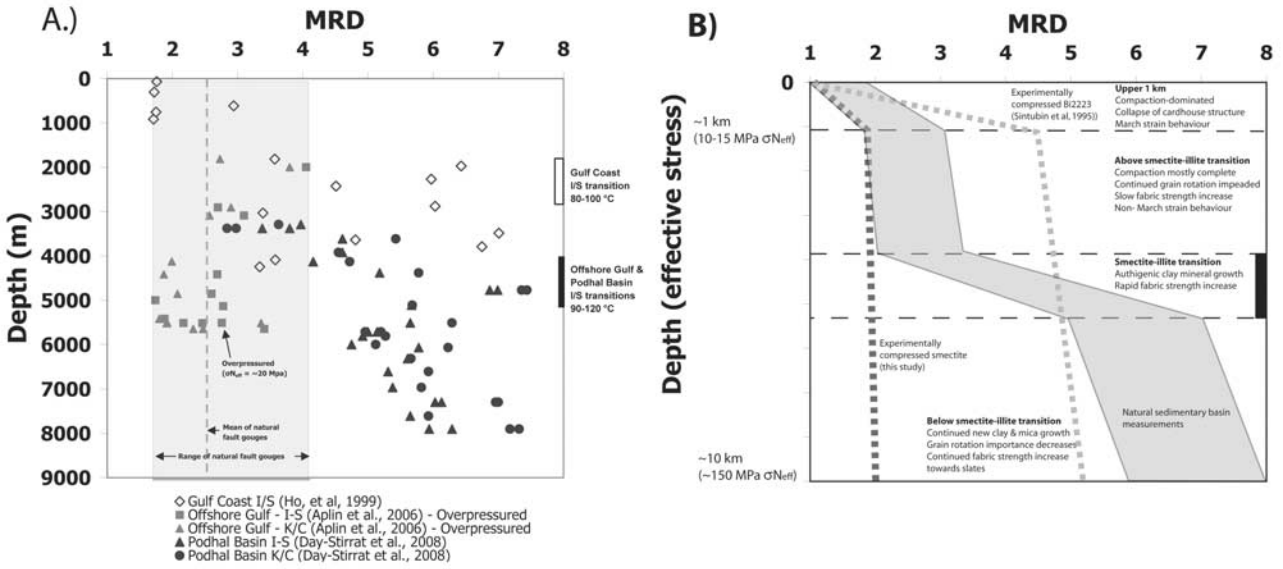

Figure 12. Comparison of published fabric intensity from sedimentary sequences with observed clay fabric intensities in clay gouges. (a) Plot of published sedimentary basin fabric intensity data showing rapid increases of fabric intensity across the smectite-illite transition in all basins. Data from *Ho et al.* [1999], *Aplin et al.* [2006], and *Day-Stirrat et al.* [2008]. (b) Schematic representation of the fabric development in shale as inferred from natural data presented in Figure 12a and experimental data from *Sintubin et al.* [1995] and this study. Grey field is fabric development in natural shales. Dashed lines are fabric measurements from experimentally compressed material (smectite is from this study, Bi2223 is from *Sintubin et al.* [1995]). *Tullis* [1976] data are not plotted, as normal stresses used during compaction are not known.

Figure 5), inconsistent with development of very large shear strains near the upper margin of Cordilleran low-angle normal fault zones.

6.1.3. Natural Clay Fabrics and Authigenic Clays

[44] Natural clay-rich fault zones show evidence for authigenic growth of clays during deformation [e.g., *Vrolijk and van der Pluijm*, 1999; *van der Pluijm et al.*, 2001; *Solum et al.*, 2005; Haines, unpublished thesis, 2008]. Measured fabric intensities for clays that are demonstrably detrital (chlorite) and fabric intensities for clays that are authigenic (illite, smectite, corrensite, sepiolite, and palygorskite), are very similar. Both types of clays in gouges have MRD's that average 2.5, ($1\sigma = 0.5$, N = 52 for detrital and $1\sigma = 0.5$, N = 93 for authigenic). Clay fabric intensity is, therefore, governed primarily by physical processes and not by chemical processes (i.e., reactions).

6.2. Implications of Experimental Clay Fabrics for Natural Gouges

6.2.1. Experimental Clay Fabric and Shear Strain

[45] The fabric intensity data from our experimental gouges indicate that the preferred orientation of phyllosilicates in clay-rich material is primarily a function of shear strain and the applied normal stress. Fabric intensity does not vary systematically with clay content. Clay fabrics appear to have developed almost completely by a shear strain of about 5, and increase only slightly with higher shear strains, suggesting that there is an "upper limit" to clay fabric intensity generated by physical granular flow processes alone. At shear strains of 3.5, slip is already concentrated along narrow R and Y surfaces, leaving the regions of P foliation as "spectator regions" of low-strain material that are transported passively in the fault [e.g., *Mair and Hazzard*, 2007] (Figure 9). The existence of spectator regions would help to preserve low fabric intensities for the gouge zone as a whole. It is possible that lack of increase of fabric intensity across natural LANF's approaching the PSP could be attributed to this process. We are at present unable to test this further by generating very high shear strains (on the order of the 10s to 100s suggested for natural LANF rocks) in the laboratory, owing to samples becoming too thin to be measured reliably using XTG. Normal stress is important in accelerating clay fabric development at a given shear strain, and it apparent, for our experimental 100% montmorillonite mixtures, that fabric intensity is sensitive to applied normal stress (Figures 9 and 10).

6.2.2. Clay Fabrics and Compaction

[46] We find that unconfined compression of smectitic material, without shear, does not produce a strong preferred orientation. This contrasts with the March model prediction [*March*, 1932] of passive particle rotation during compaction and porosity loss, which suggests that fabric intensity increases systematically with compaction. However, it is important to consider the range of stresses over which particle rotation is likely to dominate fabric development. During burial, porosity is reduced from initial values of >60% to <30% within the first kilometer or two of burial [e.g., *Athy*, 1930; *Hamilton*, 1978], where differential stresses are 1–10 MPa [e.g., *Bolwes et al.*, 1969; *Vasseur et al.*, 1995]. The differential stresses applied to the experimental gouge samples in this study (10–150 MPa) are considerably higher than those at which the majority of natural compaction occurs.

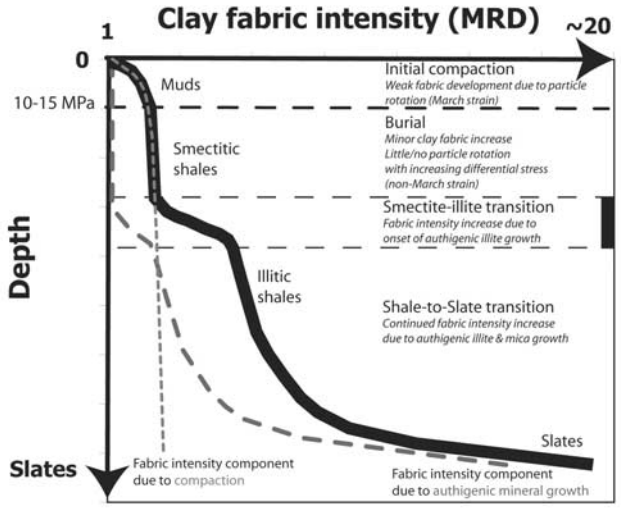

Figure 13. Schematic figure of clay fabric intensity plotted against depth showing relative contributions of compaction and authigenic mineral growth in the development of fabric intensity in diagenetic sequences as inferred from our fabric intensity measurements and previously published data. Thick line is representative fabric intensity evolution in sedimentary basins from deposition to low-grade metamorphism as inferred from natural data. Short-dashed line is component of measured fabric in sedimentary rocks due to compaction as inferred from this study, *Tullis* [1976], and *Sintubin et al.* [1995]. Long-dashed line is component of fabric in sedimentary rocks due to authigenic mineral growth.

Thus, it is likely that our experimental samples were already compressed to low porosity, even at the lowest stresses used, and that very little pore space remained for clay crystallites to rotate and further reorient with increasing normal stress. In this case, higher differential stress would not produce stronger clay fabrics at compressive stresses beyond ~10 MPa. Similar non-March strain behavior has been observed in fabric intensity measurements on compressed experimental aggregates of powdered phlogopite [*Tullis*, 1976] and Bi2223, a synthetic superconducting material ($Bi_2Sr_2Ca_2Cu_3O_x$) with a platy crystal morphology [*Sintubin et al.*, 1995]. These studies indicated that the fabric intensity of experimental aggregates increased rapidly at differential stresses lower than 10 MPa, and then rose only slightly with continued compression to >800 MPa. The phlogopite material asymptotically approached a fabric intensity of ~10.0 MRD with increasing normal stress [*Tullis*, 1976], while the Bi2223 asymptotically approached a fabric intensity of ~6.0 MRD [*Sintubin et al.*, 1995] (Figure 12). Both materials exhibited March strain behavior at low compressive stresses (below 10 MPa) and then non-March behavior at higher stresses. Thus it seems likely from both our own data and previously published results that March strain behavior may not be realistic in geologic materials at compressive stresses much above ~10 MPa.

[47] A lack of increasing fabric preferred orientation with increasing loading stress has been observed in downhole sedimentary sequences in the Gulf of Mexico and the Podhale Basin in Poland [*Ho et al.*, 1995; *Day-Stirrat et al.*, 2008]. These studies shows that fabric intensity does not increase systematically with depth (i.e., with increasing differential stress), but instead increases rapidly across the smectite-to-illite transition as a function of the growth of new minerals (e.g., Figure 12). Strong fabrics (MRD = 3–6) were found below the depths at which mineral transformations in the Gulf Coast [*Ho et al.*, 1999] and Podhale Basin sections [*Day-Stirrat et al.*, 2008], whereas for the offshore Gulf section [*Aplin et al.*, 2006], where the I/S transformation is not complete, fabrics remained low with increasing depth. The offshore Gulf section is overpressured (effective stress ~20 MPa for the entire section) whereas the Gulf Coast and Podhal basin sections are normally pressured. The Gulf Coast and Podhal examples are both clear evidence of a lack of compaction-induced fabric development with increasing effective stresses, and instead are evidence for an increase in fabric intensity due to authegenic clay growth.

[48] A key finding of our study is that prior work overestimates the role of mechanical rotation for compaction-induced fabric development in shales [e.g., *Lambe*, 1953, 1958; *Ingles*, 1968; *Yong*, 1972]. Prior work consistently depicts compaction-induced fabrics as similar to those in the "strong" clay fabric of Figure 1. However, our study quantifies clay fabric intensity directly, and shows that mechanical rotation due to compaction is not a major factor in generating preferred orientation in clay particles. The fabrics obtained by mechanical rotation due to compaction in the laboratory are weak (1.6–1.8) in comparison to those formed by compaction and shearing in the laboratory (1.9–4.6) and are much weaker than those developed by sedimentary diagenetic processes (1.8–7.6, typically 3.0–6.0; Figure 12) [*Ho et al.*, 1999; *Aplin et al.*, 2006; *Day-Stirrat et al.*, 2008].

[49] During diagenetic processes, authigenic minerals grow with a preferred orientation in response to a differential stress. Fabric evolution occurs via the transition from smectite to illite in sedimentary basins [e.g., *Ho et al.*, 1995; *Day-Stirrat et al.*, 2008] or the growth of new phyllosilicate phases during the transition from shales to slates in low-grade metamorphism [e.g., *Ho et al.*, 2001]. These data suggest that in sedimentary basins at depths above the onset of the smectite-to-illite transformation, fabric intensity is dominated by compaction, whereas at and below the smectite-to-illite transformation, fabric intensity is almost entirely dominated by authigenic (mineral-forming) processes (Figure 13). Another consideration in evaluating fabric development is the role of water in aiding grain boundary sliding in compacted samples. Our laboratory experiments were performed dry, so the role of water on aiding fabric development by grain boundary sliding could not be evaluated.

7. Conclusions

[50] We conclude that fault gouge phyllosilicate fabric intensities are uniformly weak compared to those observed in shales and slates. Clay fabric intensities of natural fault gouge do not vary significantly as a function of tectonic environment or mineralogy of the dominant clay phase. Transects across low-angle normal fault zones show that gouge clay fabrics do not increase systematically with increasing shear strain. The weakness of clay fabric intensi-

ties in natural gouges seems to rule out strongly anisotropic permeability, as required in some models for the generation of elevated fluid pressures within fault zones.

[51] XTG fabric intensity measurements from laboratory experiments with synthetic clay-quartz gouge lead to the following three main conclusions:

[52] 1. Experimental clay gouge phyllosilicate fabrics are weak, but fabric intensities vary systematically with shear strain. Fabric intensities for strained samples range from 1.7 to 4.6 and increase with increasing strain up to shear strains of ~5, after which further increases in fabric intensity are negligible. Fabric intensity in sheared samples is enhanced by increased normal stress.

[53] 2. Gouges that are subject to compressive loading without shear acquire a weak fabric, regardless of the applied normal stress. This fabric is generally developed perpendicular to the applied normal stress. Samples that are both compressed and sheared develop fabrics in which the clay crystallites are oriented obliquely, roughly 15° to σ_1, along P surfaces.

[54] 3. Samples that are compacted without shear have very weak fabrics, regardless of the applied normal stress. In light of these observations, the hypothesis that mudrocks acquire their preferred orientation primarily from compaction needs to be reconsidered, especially in environments where the differential stress is greater than 10 MPa, although the role of water saturation in aiding grain boundary sliding has not been evaluated.

[55] **Acknowledgments.** We are grateful to Susan Cashman and an anonymous reviewer for careful reviews which greatly clarified the arguments and structure of the paper. We are also grateful to John Solum and Anja Schleicher for unpublished XTG data and laboratory support, Suzanne Janecke who provided sample material from the Salton Detachment, and Darrel Cowan who introduced us to the fault rocks of the Death Valley area. This work was made possible by NSF grants EAR-0345985 and EAR-0738435 (to B.v.d.P.), EAR-0545702 (to C.M. and D.S.), and OCE-0648331 (to C.M. and D.S.) and by an AAPG Grant-in-Aid to Haines. Acknowledgment is made to the Donors of the American Chemical Society Petroleum Research Fund for partial support of this research to D.S. and C.M.

References

Aplin, A., I. Matenaar, D. McCarty, and B. van der Pluijm (2006), Influence of mechanical compaction and clay mineral diagenesis on the microfabric and pore-scale properties of deep-water Gulf of Mexico mudstones, *Clays Clay Miner.*, *54*, 500–514, doi:10.1346/CCMN.2006.0540411.

Athy, L. (1930), Density, porosity and compaction of sedimentary rocks, *Am. Assoc. Petrol. Geol. Bull.*, *14*, 1–24.

Axen, G. (2004), Mechanics of low-angle normal faults, in *Rheology and Deformation of the Lithosphere at Continental Margins*, edited by G. Karener et al., pp. 46–91, Columbia Univ. Press, New York.

Axen, G., and J. Fletcher (1998), Late Miocene-Pliocene extensional faulting, northern California, Mexico, and Salton Trough, California, *Int. Geol. Rev.*, *40*, 219–244.

Bolwes, F., W. Bryant, and C. Wallin (1969), Microstructure of unconsolidated and consolidated marine sediments, *J. Sediment. Petrol.*, *39*, 1546–1551.

Brown, K., A. Kopf, M. Underwood, and J. Weinberger (2003), Compositional and fluid pressure controls on the state of stress on the Nankai subduction thrust: A weak plate boundary, *Earth Planet. Sci. Lett.*, *214*, 589–603, doi:10.1016/S0012-821X(03)00388-1.

Buck, W. (1988), Flexural rotation of normal faults, *Tectonics*, *7*, 959–973, doi:10.1029/TC007i005p00959.

Byerlee, J. (1978), Friction of rocks, *Pure Appl. Geophys.*, *116*, 615–626, doi:10.1007/BF00876528.

Chester, F., and J. Logan (1987), Composite planer fabric of gouge from the punchbowl Fault, California, *J. Struct. Geol.*, *9*, 621–634.

Chester, F., M. Friedman, and J. Logan (1985), Foliated cataclasites, *Tectonophysics*, *111*, 139–145, doi:10.1016/0040-1951(85)90071-X.

Cladouhos, T. (1999a), Shape preferred orientations of survivor grains in fault gouge, *J. Struct. Geol.*, *21*, 419–436, doi:10.1016/S0191-8141(98)00123-0.

Cladouhos, T. (1999b), A kinematic model for deformation within brittle shear zones, *J. Struct. Geol.*, *21*, 437–448, doi:10.1016/S0191-8141(98)00124-2.

Coney, P. (1980), Cordilleran metamorphic core complexes: An overview, in *Cordilleran Metamorphic Core Complexes*, *Geol. Soc. Am. Mem.*, vol. 153, edited by M. Crittenden, pp. 7–31, Geol. Soc. of Am., Boulder, Colo.

Cowan, D. (1999), Do faults preserve a record of seismic slip? A field geologist's opinion, *J. Struct. Geol.*, *21*, 995–1001, doi:10.1016/S0191-8141(99)00046-2.

Cowan, D., T. Cladouhos, and J. Morgan (2003), Structural geology and kinematic history of rocks formed along low-angle normal faults, Death Valley, California, *Geol. Soc. Am. Bull.*, *115*, 1230–1248, doi:10.1130/B25245.1.

Crawford, B., R. Myers, A. Woronow, D. Faulkner, and E. Rutter (2002), Porosity-permeability relationships in clay-bearing fault gouge, Paper presented at the SPE/ISRM Rock Mechanics Conference, Soc. of Petrol. Eng., Irving, Texas, 20–23 Oct.

Curtis, C., S. Lipshie, G. Oertel, and M. Pearson (1980), Clay orientation is some Upper Carboniferous mudrocks, its relationship to quartz content and some inferences about fissility, porosity and compactional history, *Sedimentology*, *27*, 333–339, doi:10.1111/j.1365-3091.1980.tb01183.x.

Dallmeyer, R., A. Snoke, and E. McKee (1986), The Mesozoic-Ceneozoic tectonothermal evolution of the Ruby Mountains, East Humboldt range, Nevada: A cordilleran metamorphic core complex, *Tectonics*, *5*, 931–954, doi:10.1029/TC005i006p00931.

Davatzes, N., J. Solum, D. Lockner, and S. Stanchits (2005), Fault rock generation, frictional properties, and permeability in the Moab fault rocks, Utah, paper presented at Geological Society of America Annual Meeting 2005, Geol. Soc. of Am., Salt Lake City, abstract 226-6.

Day-Stirrat, R., A. Aplin, J. Środoń, and B. van der Pluijm (2008), Diagenetic reorientation of phyllosilicate minerals in Paleogene mudstones of the Podhale Basin, southern Poland, *Clays Clay Miner.*, *56*, 100–111, doi:10.1346/CCMN.2008.0560109.

Di Toro, G., S. Nielsen, and G. Pennacchioni (2005), Earthquake rupture dynamics frozen in exhumed ancient faults, *Nature*, *436*, 1009–1012, doi:10.1038/nature03910.

Dokka, R., M. Mahaffie, and A. Snoke (1986), Thermochronologic evidence of major tectonic denudation associated with detachment faulting, northern Ruby Mountains, East Humboldt Range, Nevada, *Tectonics*, *5*, 995–1006, doi:10.1029/TC005i007p00995.

Faulkner, D. R., and E. H. Rutter (2001), Can the maintenance of overpressured fluids in large strike-slip fault zones explain their apparent weakness?, *Geology*, *29*, 503–506, doi:10.1130/0091-7613(2001)029<0503:CTMOOF>2.0.CO;2.

Gibson, R. (1998), Physical character and fluid-flow properties of sandstone-derived fault gouge, in *Structural Geology in Reservoir Characterization*, *Geol. Soc. Spec. Publ.*, vol. 127, edited by M. Coward, pp. 87–93, Geol. Soc., Tulsa, Okla.

Hamilton, E. (1978), Sound velocity-density relations in sea-floor sediments and rocks, *Acoust. Soc. Am. J.*, *63*, 366–377.

Hayman, N. (2006), Shallow crustal faults from the Black Mountain detachments, Death Valley, CA, *J. Struct. Geol.*, *28*, 1767–1784, doi:10.1016/j.jsg.2006.06.017.

Hayman, N., B. Housen, T. Cladouhos, and K. Livi (2004), Magnetic and clast fabrics as measurements of grain-scale processes within the Death Valley shallow-crustal detachment faults, *J. Geophys. Res.*, *109*, B05409, doi:10.1029/2003JB002902.

Heilbronner, R., and C. Pauli (1993), Integrated spatial and orientation analysis of quartz c-axes by computer-aided microscopy, *J. Struct. Geol.*, *15*, 369–382, doi:10.1016/0191-8141(93)90133-U.

Ho, N., D. Peacor, and B. van der Pluijm (1995), Reorientation mechanisms of phyllosilicates in the mudstone-to-slate transition at Lehigh Gap, Pennsylvania, *J. Struct. Geol.*, *17*, 345–356, doi:10.1016/0191-8141(94)00065-8.

Ho, N., D. Peacor, and B. van der Pluijm (1996), Contrasting roles of authigenic and detrital phyllosilicates during slaty cleavage development, *J. Struct. Geol.*, *18*, 615–623, doi:10.1016/S0191-8141(96)80028-9.

Ho, N., D. Peacor, and B. van der Pluijm (1999), Preferred orientation of phyllosilicates in Gulf Coast mudstones and relation to the smectite-illite transition, *Clays Clay Miner.*, *47*, 495–504, doi:10.1346/CCMN.1999.0470412.

Ho, N., B. van der Pluijm, and D. Peacor (2001), Static recrystallization and preferred orientation of phyllosilicates: Michigamme Formation, northern Michigan, USA, *J. Struct. Geol.*, *23*, 887–893, doi:10.1016/S0191-8141(00)00162-0.

Holeywell, R., and T. Tullis (1975), Mineral reorientation and slaty cleavage in the Martinsburg formation, Lehigh Gap, Pennsylvania, *Geol. Soc. Am. Bull.*, *86*, 1296–1304, doi:10.1130/0016-7606(1975)86<1296:MRASCI>2.0.CO;2.

Housen, B., C. Richter, and B. van der Pluijm (1993), Composite magnetic anisotropy fabrics: Experiments, numerical models, and implications for the quantification of rock fabrics, *Tectonophysics*, *220*, 1–12, doi:10.1016/0040-1951(93)90219-A.

Ikari, M., D. Saffer, and C. Marone (2007), Effect of hydration state of the frictional properties of montmorillonite-based fault gouge, *J. Geophys. Res.*, *112*, B06423, doi:10.1029/2006JB004748.

Ingles, O. (1968), Soil chemistry relevant to the engineering behavior of soils, in *Soil Mechanics: Selected Topics*, edited by I. Lee, pp. 1–57, Elsevier, New York.

Jacob, G., H. Kisch, and B. van der Pluijm (2000), The relationship of phyllosilicate orientation, X-ray diffraction intensity ratios and c/b fissility ratios in metasedimentary rocks of the Helvetic zone of the Swiss Alps and the Caledonides of Jämtland, central western Sweden, *J. Struct. Geol.*, *22*, 245–258, doi:10.1016/S0191-8141(99)00149-2.

Lambe, T. (1953), The structure of inorganic soil, *Proc. Am. Soc. Civ. Eng.*, *79*, 1–49.

Lambe, T. (1958), The structure of compacted clay, *Proc. Am. Soc. Civ. Eng.*, *84*, 1–34.

Lipshie, S., G. Oertel, and J. Christie (1976), Measurement of preferred orientation of phyllosilicates in schists, *Tectonophysics*, *34*, 91–99, doi:10.1016/0040-1951(76)90178-5.

Lloyd, G. (1987), Atomic number and crystallographic contrast images with the SEM: A review of backscattered electron techniques, *Mineral. Mag.*, *51*, 3–19, doi:10.1180/minmag.1987.051.359.02.

Logan, J., and K. Rauenzahn (1987), Frictional dependence of gouge mixtures of quartz and montmorillonite on velocity, composition, and fabric, *Tectonophysics*, *144*, 87–108, doi:10.1016/0040-1951(87)90010-2.

Logan, J., M. Friedman, and M. Higgs (1979), Experimental studies of stimulated gouge and their application to studies of natural fault zones, in *Analysis of Actual Fault Zones in Bedrock*, edited by C. Dengo and T. Shimamoto, pp. 305–343, U. S. Geol. Surv., Menlo Park, Calif.

Lupini, J., A. Skinner, and P. Vaughan (1981), The drained residual strength of cohesive soils, *Geotechnique*, *31*, 181–213.

Mair, K., and J. F. Hazzard (2007), Nature of stress accommodation in sheared granular material: Insights from 3D numerical modeling, *Earth Planet. Sci. Lett.*, *259*, 469–485, doi:10.1016/j.epsl.2007.05.006.

Mair, K., and C. Marone (1999), Friction of simulated fault gouge for a wide range of velocities and normal stresses, *J. Geophys. Res.*, *104*, 28,899–28,914.

March, A. (1932), Mathematische theorie der regelung nach der korngestalt bei affiner deformation, *Z. Kristallogr. Kristallgeom. Kristallphys. Kristallchem.*, *81*, 285–297.

McGrew, A., and L. Snee (1994), $^{40}Ar/^{39}Ar$ thermochronologic constraints on the tectonothermal evolution of the northern East Humboldt Range metamorphic core complex, Nevada, *Tectonophysics*, *238*, 425–450, doi:10.1016/0040-1951(94)90067-1.

McGrew, A., M. Peters, and J. Wright (2000), Thermobarometric constraints on the tectonothermal evolution of the East Humboldt Range metamorphic core complex, Nevada, *Geol. Soc. Am. Bull.*, *112*, 45–60, doi:10.1130/0016-7606(2000)112<0045:TCOTTE>2.3.CO;2.

Miller, M. (1996), Ductility in fault gouge from a normal fault system, Death Valley, California: A mechanism for fault-zone strengthening and relevance to paleoseismicity, *Geology*, *24*, 603–606, doi:10.1130/0091-7613(1996)024<0603:DIFGFA>2.3.CO;2.

Miller, M., and L. Wright (2004), *Geology of Death Valley National Park: Landforms, Crustal Extension, Geologic History, Road Guides*, 2nd ed., 123 pp., Kendall/Hunt, Dubuque, Iowa.

Moore, D. M., and R. C. Reynolds Jr. (1997), *X-Ray Diffraction and the Identification and Analysis of Clay Minerals*, Oxford Univ. Press, New York.

Moore, D., R. Summers, and J. Byerlee (1989), Sliding behavior and deformation textures of heated illite gouge, *J. Struct. Geol.*, *11*, 329–342, doi:10.1016/0191-8141(89)90072-2.

Morrow, C., L. Q. Shi, and J. Byerlee (1984), Permeability of fault gouge under confining pressure and shear stress, *J. Geophys. Res.*, *89*, 3193–3200, doi:10.1029/JB089iB05p03193.

Morrow, C., B. Radney, and J. Byerlee (1992), Frictional strength and the effctive pressure law of montmorillonite and illite clays, in *Fault Mechanics and Transport Properties of Rocks: A Festschrift in Honor of W. F. Brace*, edited by B. Evans, pp. 69–88, Academic, San Diego, Calif.

Morrow, C., D. Moore, and D. Lockner (2000), The effect of mineral bond strength and absorbed water on fault gouge frictional strength, *Geophys. Res. Lett.*, *27*, 815–818, doi:10.1029/1999GL008401.

Mueller, K., and A. Snoke (1993), Progressive overprinting of normal fault systems and their role in Tertiary exhumation of the East Humboldt-Woods Hills metamorphic complex, northeast Nevada, *Tectonics*, *12*, 361–371, doi:10.1029/92TC01967.

Numelin, T., C. Marone, and E. Kirby (2007), Frictional properties of natural fault gouge from a low-angle normal fault, Panamint Valley, California, *Tectonics*, *26*, TC2004, doi:10.1029/2005TC001916.

O'Brien, D., H. Wenk, L. Ratschbacher, and Z. You (1987), Preferred orientation of phyllosilicates in phyllonites and ultramylonites, *J. Struct. Geol.*, *9*, 719–730, doi:10.1016/0191-8141(87)90155-6.

Oertel, G. (1983), The relationship of strain and preferred orientation of phyllosilicate grains in rocks–a review, *Tectonophysics*, *100*, 413–447, doi:10.1016/0040-1951(83)90197-X.

Oertel, G., and C. Curtis (1972), Clay-ironstone concretions preserving fabrics due to progressive compaction, *Geol. Soc. Am. Bull.*, *83*, 2597–2606, doi:10.1130/0016-7606(1972)83[2597:CCPFDT]2.0.CO;2.

Pares, J., B. van der Pluijm, and J. Dinarès-Turell (1999), Evolution of magnetic fabrics during incipient deformation of mudrocks (Pyrenees, Northern Spain), *Tectonophysics*, *307*, 1–14, doi:10.1016/S0040-1951(99)00115-8.

Pavlis, T., L. Serpa, and C. Keener (1993), Role of seismogenic processes in fault-rock development; an example from Death Valley, *Calif. Geol.*, *21*, 267–270.

Price, G. (1973), The photometric method used in microstructural analysis, *Am. J. Sci.*, *273*, 523–537.

Puigdefàbregas, C., J. Muñoz, and M. Marzo (1986), Thrust development in the eastern Pyrenees and related depositional sequences in the southern foreland basin, in *Foreland Basins*, *Int. Assoc. Sedimentol. Spec. Publ.*, vol. 8, edited by P. Allen and P. Homewood, pp. 229–246, Blackwell Sci, Oxford, U. K.

Rice, J. R. (1992), Fault stress states, pore pressure distributions, and the weakness of the San Andreas Fault, in *Fault Mechanics and Transport Properties of Rocks: A Festschrift in honor of W.F. Brace*, edited by B. Evans and T.-F. Wong, pp. 475–503, Academic, San Diego, Calif.

Richter, C., B. van der Pluijm, and B. Housen (1993), The quantification of crystallographic preferred orientation using magnetic anisotropy, *J. Struct. Geol.*, *15*, 113–116, doi:10.1016/0191-8141(93)90082-L.

Saffer, D., and C. Marone (2003), Comparison of smectite- and illite-rich gouge frictional properties: Application to the updip limit of the seismogenic zone along subduction megathrusts, *Earth Planet. Sci. Lett.*, *215*, 219–235, doi:10.1016/S0012-821X(03)00424-2.

Saffer, D., K. Frye, C. Marone, and K. Mair (2001), Laboratory results indicating complex and potentially unstable frictional behavior of smectite clay, *Geophys. Res. Lett.*, *28*, 2297–2300, doi:10.1029/2001GL012869.

Schleicher, A., B. van der Pluijm, J. Solum, and L. Warr (2006), Origin and significance of clay-coated fractures in mudrock fragments of the SAFOD borehole (Parkfield California), *Geophys. Res. Lett.*, *33*, L16313, doi:10.1029/2006GL026505.

Schleicher, A., L. Warr, and B. van der Pluijm (2009), On the origin of mixed-layered clay minerals from the San Andreas Fault at 2.5–3 km vertical depth (SAFOD) drillhole at Parkfield, California), *Contrib. Mineral. Petrol.*, doi:10.1007/s00410-008-0328-7, in press.

Schulz, L (1949), Determination of preferred orientation in flat transmission samples using a Geiger Counter X-ray spectrometer, *J. Appl. Phys.*, *20*, 1033–1036, doi:10.1063/1.1698269.

Sibson, R. (1977), Fault rocks and fault mechanisms, *J. Geol. Soc.*, *133*, 191–213, doi:10.1144/gsjgs.133.3.0191.

Sintubin, M. (1994a), Phyllosilicate preferred orientation in relation to strain path determination in the lower Paleozoic Stavelot-Venn Massif (Ardennes, Belgium), *Tectonophysics*, *237*, 215–231, doi:10.1016/0040-1951(94)90256-9.

Sintubin, M. (1994b), Clay fabrics in relation to the burial history of shales, *Sedimentology*, *41*, 1161–1169, doi:10.1111/j.1365-3091.1994.tb01447.x.

Sintubin, M., H.-R. Wenk, and D. Phillips (1995), Texture development in platy materials: Comparison of Bi2223 aggregates with phyllosilicate fabrics, *Mater. Sci. Eng. A*, *202*, 157–171, doi:10.1016/0921-5093(95)09811-9.

Snoke, A. (1980), Transition from infrastructure to superstructure in the Northern Ruby Mountains, Nevada, in *Cordilleran Metamorphic Core Complexes*, *Geol. Soc. Am. Mem.*, vol. 153, edited by M. Crittenden, pp. 287–333, Geol. Soc. of Am., Boulder, Colo.

Snoke, A., and K. Howard (1984), Geology of the Ruby Mountains-East Humboldt Range, Nevada: A Cordilleran metamorphic core complex, in *Western Geological Excursions*, edited by J. Lintz, pp. 260–303, Mackay Sch. of Mines, Reno, Nev.

Solum, J., B. van der Pluijm, D. Peacor, and L. Warr (2003), Influence of phyllosilicate mineral assemblages, fabrics and fluids on the behavior of the Punchbowl Fault, southern California, *J. Geophys. Res.*, *108*(B5), 2233, doi:10.1029/2002JB001858.

Solum, J., B. van der Pluijm, and D. Peacor (2005), Neocrystallization, fabrics and age of clay minerals from an exposure of the Moab Fault, Utah, *J. Struct. Geol.*, *27*, 1563–1576, doi:10.1016/j.jsg.2005.05.002.

Storti, F., A. Billi, and F. Salvini (2003), Particle size distributions in natural carbonate fault rocks: Insights for non-self-similar cataclasis, *Earth Planet. Sci. Lett.*, *206*, 173–186, doi:10.1016/S0012-821X(02)01077-4.

Sussman, A., R. Butler, J. Dinarès-Turell, and J. Verges (2004), Vertical-axis rotation of a foreland fold and implications for orogenic curvature: An example from the Southern Pyrenees, Spain, *Earth Planet. Sci. Lett.*, *218*, 435–449, doi:10.1016/S0012-821X(03)00644-7.

Tullis, T. (1976), Experiments on the origin of slaty cleavage and schistosity, *Geol. Soc. Am. Bull.*, *87*, 745–753, doi:10.1130/0016-7606(1976)87<745:EOTOOS>2.0.CO;2.

Tullis, T., and D. Wood (1975), Correlation of finite strain from both reduction bodies and preferred orientation of mica in slate from Wales, *Geol. Soc. Am. Bull.*, *86*, 632–638, doi:10.1130/0016-7606(1975)86<632:COFSFB>2.0.CO;2.

Turner, F., and L. Weiss (1963), *Structural Analysis of Metamorphic Tectonites*, 545 pp., McGraw-Hill, New York.

van der Pluijm, B., N. Ho, and D. Peacor (1994), High-resolution X-ray texture goniometry, *J. Struct. Geol.*, *16*, 1029–1032, doi:10.1016/0191-8141(94)90084-1.

van der Pluijm, B., C. Hall, P. Vrolijk, D. Pevear, and M. Covey (2001), The dating of shallow faults in the Earth's crust, *Nature*, *412*, 172–175, doi:10.1038/35084053.

Vasseur, G., I. Djeran-Maigre, D. Grunberger, G. Rousset, D. Tessier, and B. Velde (1995), Evolution of structural and physical parameters of clays during experimental compaction, *Mar. Petrol. Geol.*, *12*, 941–954.

Vrolijk, P., and B. van der Pluijm (1999), Clay gouge, *J. Struct. Geol.*, *21*, 1039–1048, doi:10.1016/S0191-8141(99)00103-0.

Wenk, H. (1985), Measurements of pole figures, in *Preferred Orientation in Deformed Metals and Rocks*, edited by H. Wenk, pp. 11–47, Academic, Orlando, Fla.

Wenk, H. (2006), Neutron diffraction texture analysis, *Rev. Mineral.*, *63*, 399–426, doi:10.2138/rmg.2006.63.15.

Wernicke, B., and G. Axen (1988), On the role of isostasy in the evolution of low-angle normal fault systems, *Geology*, *16*, 848–851, doi:10.1130/0091-7613(1988)016<0848:OTROII>2.3.CO;2.

Wilkinson, A., and P. Hirsch (1997), Electron diffraction based techniques in scanning electron microscopy of bulk materials, *Micron*, *28*, 279–308, doi:10.1016/S0968-4328(97)00032-2.

Yan, Y., B. van der Pluijm, and D. Peacor (2001), Deformational microfabrics of clay gouge, Lewis Thrust, Canada: A case for fault weakening from clay transformation, in *The Nature and Tectonic Significance of Fault Zone Weakening*, *Geol. Soc. Spec. Publ.*, vol. 186, edited by R. E. Holdsworth, pp. 103–112, Geol. Soc., Tulsa, Okla.

Yang, Y., and A. Aplin (2007), Permeability and petrophysical properties in 30 natural mudstones, *J. Geophys. Res.*, *112*, B03206, doi:10.1029/2005JB004243.

Yong, R. (1972), Soil technology and stabilization, paper presented at 4th Asian Regional Conference on Soil Mechanics and Foundation Engineering 2, Asian Technol. Inst., Bangkok, 26 July to 1 Aug.

Zhang, S., and S. Cox (2000), Enhancement of fluid permeability during shear deformation of a synthetic mud, *J. Struct. Geol.*, *22*, 1385–1393, doi:10.1016/S0191-8141(00)00065-1.

S. H. Haines and B. A. van der Pluijm, Department of Geological Sciences, University of Michigan, 1100 North University Avenue, 2534 C.C. Little Building, Ann Arbor, MI 48109, USA. (shhaines@umich.edu)

M. J. Ikari, C. Marone, and D. M. Saffer, Department of Geosciences and Energy Institute Center for Geomechanics, Geofluids, and Geohazards, Penn State University, 522 Deike Building, University Park, PA 16802, USA.